

**CSDL-T-1227**

**PERFORMANCE ANALYSIS OF AN  
INTEGRATED GPS/INERTIAL  
ATTITUDE DETERMINATION SYSTEM**

**by**  
**Wendy I. Sullivan**

**May 1994**

**Master of Science Thesis  
Massachusetts Institute of Technology**

(NASA-CR-188289) PERFORMANCE  
ANALYSIS OF AN INTEGRATED  
GPS/INERTIAL ATTITUDE DETERMINATION  
SYSTEM M.S. Thesis - MIT (Draper  
(Charles Stark) Lab.) 91 p

N94-32864

Unclas

G3/04 0011932



The Charles Stark Draper Laboratory, Inc.  
555 Technology Square, Cambridge, Massachusetts 02139-3563



# Performance Analysis of an Integrated GPS/Inertial Attitude Determination System

by

Wendy I. Sullivan

B.S.S.E., United States Naval Academy  
(1987)

Submitted to the Department of Aeronautics and Astronautics in partial  
fulfillment of the requirements for the Degree of

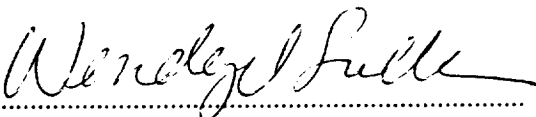
Master of Science in Aeronautics and Astronautics

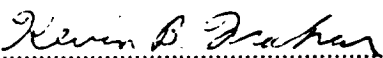
at the

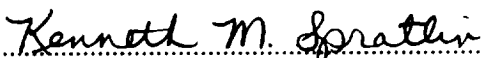
MASSACHUSETTS INSTITUTE OF TECHNOLOGY

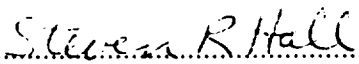
May 1994

© Wendy I. Sullivan, 1994. All Rights Reserved.

Signature of Author .....   
Department of Aeronautics and Astronautics  
May 1994

Approved by .....   
Kevin B. Mahar  
Senior Member Technical Staff, Charles Stark Draper Laboratory, Inc.  
Technical Supervisor

Approved by .....   
Kenneth M. Spratlin  
Senior Member Technical Staff, Charles Stark Draper Laboratory, Inc.  
Technical Supervisor

Certified by .....   
Professor Steven R. Hall  
Department of Aeronautics and Astronautics  
Thesis Supervisor

Accepted by .....  
Professor Harold Y. Wachman  
Chairman, Department Graduate Committee



# **Performance Analysis of an Integrated GPS/Inertial Attitude Determination System**

by

Wendy I. Sullivan

Submitted to the Department of Aeronautics and Astronautics on May 19, 1994, in partial fulfillment of the requirements for the Degree of Master of Science in Aeronautics and Astronautics.

## **ABSTRACT**

The performance of an integrated GPS/inertial attitude determination system is investigated using a linear covariance analysis. The principles of GPS interferometry are reviewed, and the major error sources of both interferometers and gyroscopes are discussed and modeled. A new figure of merit, Attitude Dilution of Precision (ADOP), is defined for two possible GPS attitude determination methods, namely single difference and double difference interferometry. Based on this figure of merit, a satellite selection scheme is proposed. The performance of the integrated GPS/inertial attitude determination system is determined using a linear covariance analysis. Based on this analysis, it is concluded that the baseline errors (i.e., knowledge of the GPS interferometer baseline relative to the vehicle coordinate system) are the limiting factor in system performance. By reducing baseline errors, it should be possible to use lower quality gyroscopes without significantly reducing performance. For the cases considered, single difference interferometry is only marginally better than double difference interferometry. Finally, the performance of the system is found to be relatively insensitive to the satellite selection technique.

Thesis Supervisor: Professor Steven R. Hall

Title: Associate Professor,  
Department of Aeronautics and Astronautics

Technical Supervisor: Kevin B. Mahar

Title: Senior Member Technical Staff, C. S. Draper Laboratory, Inc.

Technical Supervisor: Kenneth M. Spratlin

Title: Senior Member Technical Staff, C. S. Draper Laboratory, Inc.

**PRECEDING PAGE BLANK NOT FILMED**

PAGE 3 INTENTIONALLY BLANK



# Acknowledgments

I would like to express my gratitude to all those who have supported me throughout the course of my graduate work at MIT and particularly those who have had a part in the creation of this thesis.

I especially thank Kevin Mahar and Ken Spratlin for their expertise, their help and patience as my technical advisors.

I thank Professor Steve Hall for his time and advice, his inputs greatly improved the final thesis.

I also thank all the members of the technical staff at Draper who have made my experience here both challenging and enjoyable, including Stan Sheppard, Doug Fuhry, and Tony Bogner.

I thank Greg and Tony for the reference help; I couldn't have made it without you!

I thank Karen and Santo for their invaluable help with writing and editing.

I thank Tom and Karen Fitzgerald for keeping me in their thoughts, and making sure I got away from the computer once in a while.

I thank all the other Draper Fellows who have contributed to my MIT experience, Marc, Fred, Mike, Rob, John, Jeff, and especially Lisa. I especially grateful to Lisa for her encouragement, her chocolate chip cookies, and most of all her friendship.

I thank my Mom, for all her encouragement.

And, I thank my husband, Jim, whose love and understanding have made everything else worthwhile.

This thesis was prepared at the Charles Stark Draper Laboratory, Inc., under NASA Contract # NAS9-18426.

Publication of this thesis does not constitute approval by the Draper Laboratory or the sponsoring agency of the findings or conclusions contained herein. It is published for the exchange and stimulation of ideas.

I hereby assign my copyright of this thesis to the Charles Stark Draper Laboratory, Inc., Cambridge, Massachusetts.

---

Wendy I. Sullivan

Permission is hereby granted by The Charles Stark Draper Laboratory, Inc. to the Massachusetts Institute of Technology to reproduce any or all of this thesis.



# Table of Contents

Chapter	Page
1 Introduction.....	13
1.1 Motivation .....	13
1.2 GPS Interferometry .....	14
1.3 Performance Factors .....	17
1.4 Thesis Objectives .....	18
2 Error Sources and Modeling .....	19
2.1 Gyroscope/Interferometer Configuration .....	19
2.2 GPS Error Sources .....	19
2.2.1 Phase Error .....	20
2.2.2 Multipath .....	20
2.2.3 Flexures .....	22
2.2.4 Propagation Errors .....	23
2.2.5 Clock Errors .....	24
2.2.6 Path Delay .....	24
2.2.7 Integer Ambiguity and Cycle Slip .....	24
2.2.8 Satellite Geometry .....	26
2.3 Gyroscope Errors .....	27
2.3.1 Bias .....	27
2.3.2 Scale Factor Error .....	27
2.3.3 Misalignment .....	27
2.3.4 Angle Random Walk .....	28
2.4 GPS Error Models .....	28
2.5 Gyroscope Error Models .....	30
3 Satellite Selection.....	31
3.1 Introduction .....	31
3.2 Attitude Dilution of Precision .....	31
3.2.1 Variations and Extensions of ADOP .....	33
3.2.2 Single Difference Sensitivities .....	33
3.2.3 Double Difference Sensitivities .....	35
3.2.4 Sample Calculations of ADOP .....	36
3.3 Pitch and Yaw Sensitivities .....	39
4 Linear Covariance Analysis.....	41
4.1 Overview .....	41
4.2 Simulation .....	44
4.3 Implementation .....	46
4.3.1 Process Dynamics .....	46
4.3.1.1 Attitude Errors and Gyroscope Dynamics .....	47
4.3.1.2 Baseline Errors, Path Delays, and Multipath .....	48

4.3.2	Measurement Updates .....	48
4.3.2.1	Single Difference Measurements .....	49
4.3.2.2	Double Difference Measurements .....	49
5	Results .....	51
5.1	Performance Factors and Nominal Conditions .....	51
5.1.1	Performance Factors .....	51
5.1.2	Nominal Run Conditions .....	52
5.2	Results for the Nominal Run .....	55
5.2.1	Attitude Error .....	55
5.2.2	Baseline Errors .....	56
5.2.3	Multipath Errors .....	59
5.2.4	Path Delays .....	60
5.2.5	Gyroscope Errors .....	61
5.3	Results .....	63
5.3.1	Satellite Selection Routine .....	64
5.3.2	Measurement Type .....	64
5.3.3	Baseline Errors .....	65
5.3.4	Multipath .....	66
5.3.4.1	Multipath Level.....	69
5.3.4.2	Multipath Correlation.....	69
5.3.5	Inclination .....	70
5.3.6	Attitude Hold .....	71
5.3.7	Gyroscope Quality .....	75
6	Conclusions and Suggestions for Future Work.....	79
6.1	Conclusions .....	79
6.2	Future Work .....	80

<b>Appendix</b>	<b>Page</b>
A Geometric Dilution of Precision (GDOP) .....	81
B Derivation of Pitch and Yaw Sensitivity Equations .....	83
C The Dynamics and Process Noise Matrices .....	85
D Derivation of the Sensitivity Vectors .....	89

# List of Figures

<b>Figure</b>		<b>Page</b>
Figure 1.1	GPS Signal Arrives at Two Antennas.....	15
Figure 1.2	Double Differencing .....	16
Figure 2.1	LVLH Coordinate Frame Definition.....	20
Figure 2.2	Signal Multipath.....	21
Figure 2.3	Flexures Cause Apparent Change in Baseline Length and Orientation.....	23
Figure 2.4	Angular Effect of the Integer Ambiguity .....	25
Figure 2.5	Scale Factor Error .....	27
Figure 3.1	Satellite Geometry.....	37
Figure 3.2	ADOP Changes With Satellite Geometry .....	38
Figure 3.3	Pitch and Yaw Sensitivities.....	39
Figure 4.1	Simulation Flow Chart .....	45
Figure 5.1	Effect of GPS Measurement Rate on Attitude Errors .....	54
Figure 5.2	Nominal Case Attitude Errors.....	57
Figure 5.3	Baseline Errors .....	58
Figure 5.4	Nominal Case Multipath Error.....	59
Figure 5.5	Multipath Error .....	60
Figure 5.6	Path Delay for Baseline 1.....	61
Figure 5.7	Nominal Case Gyroscope Errors.....	62
Figure 5.8	Attitude Errors due to Different Baseline Error Levels .....	66
Figure 5.9	Baseline 1 Errors .....	67
Figure 5.10	Baseline 2 Errors .....	68
Figure 5.11	Number of Satellites Visible During a Polar Orbit .....	71
Figure 5.12	Attitude Errors for all Attitude Hold Cases .....	72
Figure 5.13	Attitude Errors During Maneuvers .....	73
Figure 5.14	Attitude Errors Caused by Loss of Satellite Visibility.....	74
Figure 5.15	Number of Satellites Visible While in an Inertial Attitude Hold.....	74
Figure 5.16	Attitude Errors for Good and Poor Quality Gyroscope .....	76
Figure 5.18	Gyro Bias Estimation for a Poor Quality Gyroscope.....	76
Figure 5.17	Comparison of Baseline Errors for Good and Poor Quality Gyros .....	77



# List of Tables

Table		Page
Table 4.1	GPS Satellite Constellation.....	46
Table 4.2	Elements of The Error State Vector.....	47
Table 5.1	Performance Factors .....	52
Table 5.2	Nominal Run Conditions .....	53
Table 5.3	Attitude Errors for the Nominal Case .....	56
Table 5.4	Gyroscope Errors .....	63
Table 5.5	Satellite Selection Routine Performance .....	64
Table 5.6	Measurement Types .....	65
Table 5.7	System Settling Times .....	65
Table 5.8	Multipath Level.....	69
Table 5.9	Multipath Correlation .....	70
Table 5.10	Orbital Inclination.....	70
Table 5.11	Performance for Attitude Hold Cases.....	72
Table 5.12	Maneuver History .....	75
Table 5.13	Gyroscope Quality Results .....	75



# Chapter 1

## Introduction

### 1.1 Motivation

Attitude determination is a vital function for all spacecraft. Accuracy requirements are often very strict to accommodate precise pointing applications. The sensors currently used for attitude determination include star trackers, sun sensors, and gyroscopes. A common configuration is comprised of high accuracy gyroscopes and star trackers. The gyroscopes are used to provide continuous data, but because all gyroscopes are subject to drift, star trackers or other sensors are needed as an inertial reference to realign the gyroscopes periodically. GPS interferometry may be used as that inertial attitude reference. With the increasing use of GPS for navigation, interferometry may be added with only a small incremental cost and change, as opposed to adding completely separate system, such as a star tracker.

GPS interferometry uses carrier phase measurements to determine vehicle attitude. Phase measurements are made at two or more antennas, and then differenced to produce a precise measurement of the direction to the GPS satellite relative to the baseline connecting the antennas. This measurement is then combined with the vehicle and GPS satellite positions to produce an inertial attitude measurement.

The use of GPS interferometry for space vehicle attitude determination is not a new idea. Tests of airborne and ground based GPS interferometers have indicated that accuracy sufficient for many space applications is possible with the current technology [9, 18]. Trimble and Loral recently announced that they will team to develop a space-qualified receiver capable of performing vehicle attitude determination. Also, GPS is

being incorporated into the attitude determination system for the International Space Station.

Stand-alone GPS attitude determination systems have been developed for marine and other earth-based applications [5, 9]. Typically, attitude measurements are only available at about 1 Hz, and no measurement is available if the GPS receiver is unable to maintain track on the signals of a sufficient number of satellites. This is not acceptable for space vehicle navigation, where continuous attitude estimates are often required. If the GPS interferometer is coupled with a gyroscopic attitude reference system, then the latter provides continuous data output and stability during short periods of high dynamics. Integration of GPS interferometers with gyroscopes has been proposed for a variety of applications, including autonomous space vehicle navigation [24], and vehicle attitude determination [2, 9], including spacecraft [6, 23]. Because GPS provides an inertial reference at every measurement, it is not necessary for the gyroscopes to maintain accuracy for long periods of time. Therefore, a GPS/inertial system could make use of smaller, cheaper gyroscopes than are currently used in most space applications.

An overview of the principles of GPS interferometry is presented in the next section, followed by a discussion of the major performance factors which are addressed in this thesis. Finally, the goals and organization of this thesis are described.

## **1.2 GPS Interferometry**

As shown in Figure 1.1, attitude determination using GPS is accomplished by measuring the difference in carrier phase as the signal arrives at two separate antennas. The total phase difference consists of a fractional part,  $\Delta\phi$ , which is often referred to as the phase difference, and a number of whole wavelengths,  $n$ , called the integer ambi-



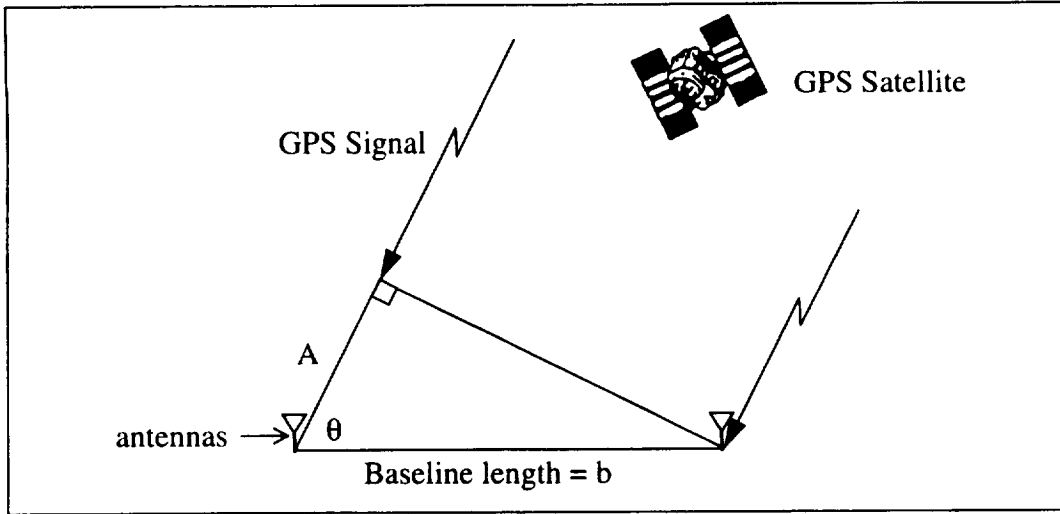


**Figure 1.1 GPS Signal Arrives at Two Antennas**

guity. Only the fractional part is measured because the integer ambiguity is not observable. Once computed, the integer ambiguity acts as a bias. It will be discussed further in Chapter 2. The total phase difference is related to the range difference from the satellite to each of the antennas (leg A of the triangle shown) by

$$A = \left(n + \frac{\Delta\phi}{2\pi}\right) \lambda \quad (1.1)$$

where  $\lambda$  is the known carrier wavelength. The phase difference measurement is called a single difference (SD).

The orientation of the antenna baseline in inertial space relative to the line of sight (LOS) to a satellite is the angle  $\theta$ , which is related to the phase difference and ambiguity by

$$\cos\theta = \left(n + \frac{\Delta\phi}{2\pi}\right) \frac{\lambda}{b} = \underline{u}_b \cdot \underline{u}_R \quad (1.2)$$

where  $\underline{u}_b$  is a unit vector along the baseline, and  $\underline{u}_R$  is a unit vector along the LOS to the satellite. In general, the resolution of  $\theta$  improves as the baseline gets longer.

Determination of the three dimensional baseline orientation in space is equivalent to the calculation of the coordinates of the baseline vector,  $\underline{b}$ . Since there are three unknowns, three independent SD measurements are required to completely determine the orientation. The phase difference measurements are not sensitive to vehicle roll about the axis of the baseline; therefore, at least two baselines are needed to determine the three dimensional attitude of a vehicle in space.

Interferometry may also be accomplished using double differences (DD) or triple differences (TD). The DD technique involves differencing phase difference measurements from two satellites (see Figure 1.2). Notice that the notation for a single difference is  $\Delta$ , which has one vertex on top (for the one satellite in the sky), and two vertices on the bottom (for the two antennas). The notation for a double difference,  $\nabla$ , has two vertices on top, representing the two satellites used for the measurement. With the DD technique, some common mode receiver errors cancel; however, an additional satellite is required, since four satellites are needed to get three independent measurements. Triple differencing involves differencing DD measurements from one time

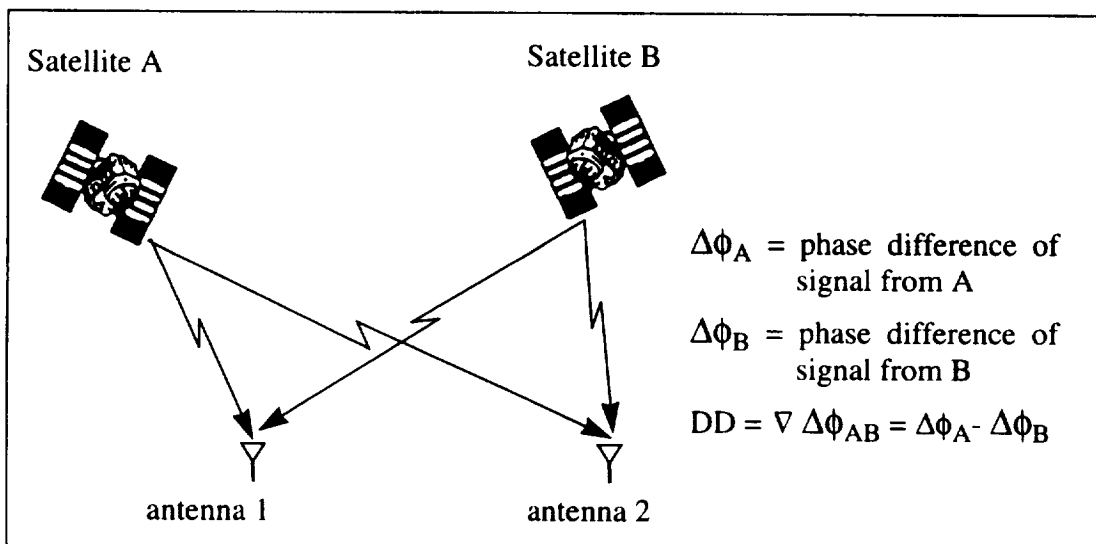


Figure 1.2 Double Differencing

period to the next. TD measurements can be used to eliminate the integer ambiguity [14, 16].

### 1.3 Performance Factors

One important aspect of implementing GPS interferometry is satellite selection [5]. From low earth orbit, there are often as many as 10 or 11 satellites in view. All-in-view-processing, which is becoming more common as advances in receivers are made, requires much more additional hardware for attitude determination than for positioning, and is not currently affordable for most applications.

The optimal satellite geometry for attitude determination is not the same as that for positioning [13]. Therefore, the dilution of precision ( $\bar{DOP}$ ) metrics defined for positioning, such as geometric dilution of precision (GDOP) and position dilution of precision (PDOP), are not valid for attitude determination. Although satellite selection schemes for pointing applications have been presented [11, 14], no instantaneous figure of merit for three dimensional attitude determination has been defined.

Another important factor is the measurement type. Double differences seem to be the most common type [3, 5, 9, 22], possibly because they are traditionally used in surveying and other differential GPS applications. In these applications, long baselines are employed, and DD are used in order to eliminate the offset between the receiver clocks which exists because separate receivers are used to make measurements at each antenna. In attitude determination, all of the phase measurements are made in reference to a common oscillator in a single receiver, so there is no receiver clock error [1, 18]. Double differences can be useful in attitude determination, because there may be differences in the electrical path length between each antenna and the receiver [1, 5, 18]. These path delays are common to all satellites being tracked, and therefore cancel

out in double difference measurements. However, there are disadvantages in using double differences, because the measurement noise level is increased by combining the measurements, and more satellites are required to obtain the same number of measurements.

## **1.4 Thesis Objectives**

This thesis will develop a model and linear covariance simulation of a coupled GPS/inertial system for a space vehicle in low earth orbit. Performance characteristics of the coupled system will be investigated for both good and poor quality gyroscopes. The effects of using single difference instead of double difference measurements will also be investigated. A definition of attitude dilution of precision (ADOP) will be developed, and the performance of various satellite selection schemes will be compared.

The thesis is organized as follows. Chapter 2 discusses the major error sources for both GPS interferometers and gyroscopes. Models for the errors included in the simulation are presented and explained. Chapter 3 presents details of the satellite selection routines. ADOP is derived, and sample calculations are presented. In Chapter 4, the details of a linear covariance analysis are provided. The implementation used in this thesis is described, and a flow chart of the simulation is presented. Performance results are presented and discussed in Chapter 5. In Chapter 6, a summary of the thesis is presented, and conclusions are drawn from the results. Suggestions for future study are also discussed.

## Chapter 2

### Error Sources and Modeling

Both GPS interferometers and gyroscopes are subject to errors from a number of sources. These errors can affect the performance of the GPS/inertial attitude determination system. For this reason, it is important to understand the sources of the errors. This chapter first describes the gyroscope/interferometry configuration with respect to the vehicle and the flight attitude. Subsequently, it discusses the principal errors that affect GPS/inertial systems, and lays out the technique that was used to model them for this analysis.

#### 2.1 Gyroscope/Interferometer Configuration

The mounting configuration between the interferometer and the gyroscopes was modeled as a rigid attachment, disregarding any flexures that may exist between the two. The baselines of the interferometer are orthogonally aligned along the x- and y-axes of the vehicle body.

The LVLH coordinate frame is defined in a non-traditional manner for this discussion with the z-axis aligned along the inertial position vector, as illustrated in Figure 2.1

#### 2.2 GPS Error Sources

GPS interferometer errors are discussed in detail below, along with their effect on attitude measurement. Any compensation techniques that can be used to reduce the errors are also described.

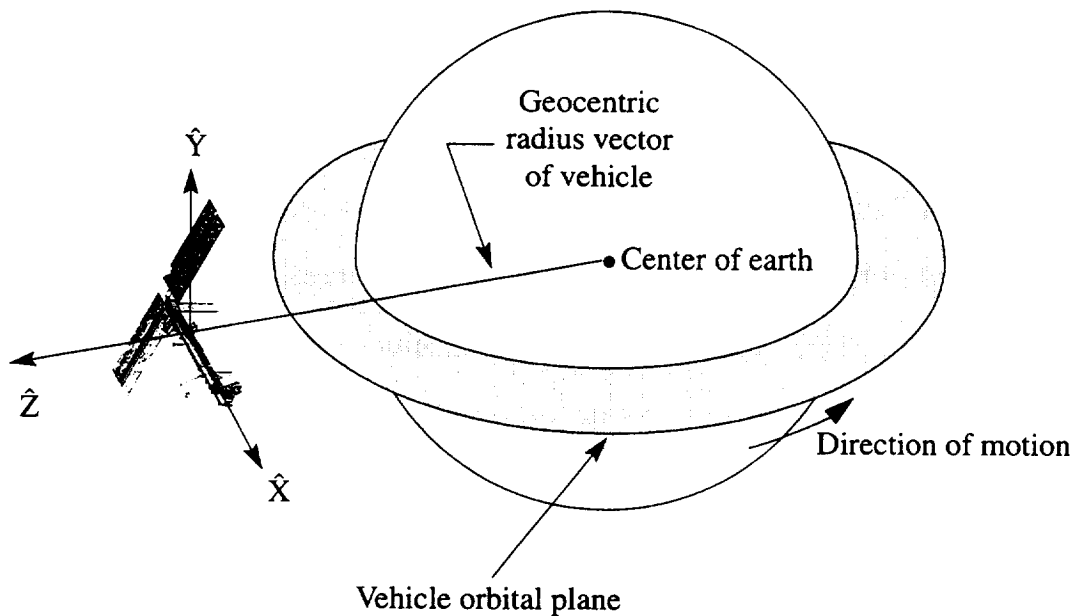


**Figure 2.1 LVLH Coordinate Frame Definition**

### **2.2.1 Phase Error**

Phase error is the error made by the receiver when it computes the phase angle of the incoming signal. Phase error depends mostly on the quality of the receiver and frequency of the output, but may also be affected by high vehicle dynamics if the vehicle dynamics are not within the tracking loop bandwidth. If the GPS tracking loops are inertially aided (as in a coupled system), then normal spacecraft dynamics will not contribute to phase error.

### **2.2.2 Multipath**

Multipath is caused by reflecting surfaces near the antenna which cause the signal to arrive at the antenna via more than one path, or worse yet, via only a non-direct path (see Figure 2.2). Multipath errors tend to be less severe in attitude determination applications, because the measurement is a difference between two closely spaced anten-

nas. Therefore, the majority of multipath signals are “common mode,” i.e., they affect both antennas equally. “Differential mode” multipath does not cancel, and tends to increase as the baselines get longer.

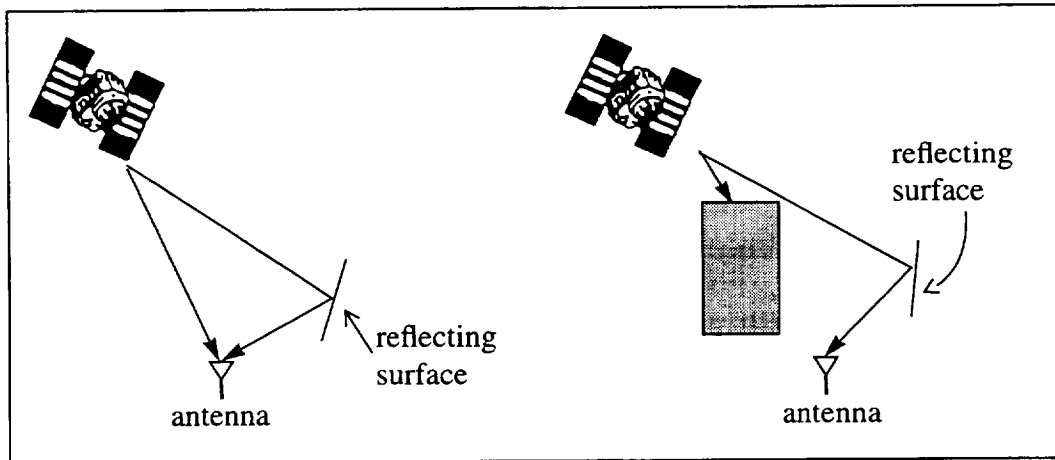


**Figure 2.2 Signal Multipath**

Multipath errors can be limited in several ways, including careful antenna placement on the vehicle, appropriate choice of antenna gain pattern and axial ratio, the use of choke rings, and coupling the GPS with a gyroscopic attitude reference system. Antennas should not be mounted near obvious sources of multipath. Most multipath enters the antenna at low elevation angles, so an antenna with a gain pattern which has low gain in this area will be less susceptible to multipath. Choke rings can also be used to mask signals which would enter the antenna at low elevation angles.

Axial ratio refers to an antenna’s sensitivity to signal polarization. All broadcast GPS signals have the same polarization, which becomes reversed if the signal reflects off another surface. By attenuating signals with incorrect polarization, the effect of most multipath signals will be minimized. Of course, signals which have reflected off of two surfaces would not be rejected in this way, but will usually be significantly attenuated by the multiple reflections.

When GPS signals corrupted with multipath are used in the attitude solution, it appears that an antenna or baseline has moved or rotated from its true orientation. If the multipath signal is being reflected off of the surface on which the antennas are mounted, then the apparent rotation will vary slowly as a sinusoid which is related to the repeating geometry of the satellite line of sight with respect to the antenna, and the reflecting object. This type of error is very difficult to distinguish from actual vehicle motion. Fortunately, most multipath of this type is common mode multipath, and cancels out in the phase difference measurement. The remaining multipath can possibly be estimated and calibrated, as previously described [4].

An object which passes too close to the antenna array, for example, the Shuttle Remote Manipulator System, or another spacecraft performing docking or rendezvous procedures, could cause either common mode or differential mode multipath. This type of multipath may begin and end abruptly as the object moves past the antenna array, causing severe errors in the attitude solution. However, if the GPS interferometer is coupled with gyroscopes, then the latter will provide a record of vehicle rotations, and it is possible to discount signals which indicate a sudden vehicle rotation which is inconsistent with the gyroscope state.

### **2.2.3 Flexures**

There are two types of flexures which can limit the accuracy of a GPS attitude determination system: flexures of the antenna baseline, and structural flexures between the baseline and the navigation base of the vehicle. The first case is illustrated in Figure 2.3. It is possible to estimate the change in baseline length [2], but the change in orientation is difficult to distinguish from vehicle rotation. This type of flexure can be minimized by keeping the baseline as short as possible.



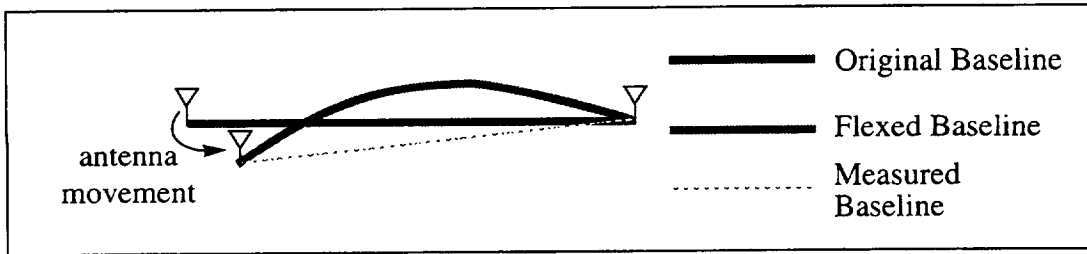


**Figure 2.3 Flexures Cause Apparent Change in Baseline Length and Orientation**

Flexures between the antenna baseline and the navigation base cause changes in the orientation of the baseline with respect to the orientation of the vehicle. Both types of flexures can be caused by thermal expansion which may occur when the spacecraft passes in and out of the earth's shadow, and by any stresses which occur during launch.

### **2.2.4 Propagation Errors**

GPS signals are refracted and delayed as they pass through the atmosphere, resulting in propagation errors. The two parts of the atmosphere which cause propagation errors are the troposphere, which extends up to about 100 km, and the ionosphere, which extends from 100 km to 1000 km above the earth's surface. Spacecraft in low earth orbit, which are considered in this thesis, operate in the ionosphere. Thus all GPS signals received by such spacecraft are subject to ionospheric refraction and retardation. In addition, measurements through the earth's limb are also subject to tropospheric errors. However, in attitude determination, the signal travels very nearly identical paths to reach each antenna, and virtually all atmospheric delays cancel out when the phase difference is computed. Signal refraction does not cancel, but the total bending through the atmosphere is only about  $0.003^\circ$  [25], and this effect is negligible compared to other error sources.

### **2.2.5 Clock Errors**

Clock errors exist in both the GPS space segment and user clocks. When the phase difference between signals from the same satellite is calculated, the bulk of these errors cancel out. The small satellite clock error which remains due to the different transmission times of the signals which arrive at the separate antennas is on the order of  $10^{-20}$  seconds for the highly accurate satellite clocks, and is not significant compared to the other error sources. Since all phase measurements are made against a common oscillator, user clock errors also cancel out.

### **2.2.6 Path Delay**

Temperature differences in the cabling and electronics result in a difference in electrical path lengths between each antenna and the receiver. The path delay is sometimes called the “apparent user clock bias” because it resembles the bias seen in Differential GPS applications when the phase measurements are made on different receivers (and therefore not relative to a common oscillator.) The path delay may be eliminated by using the double differencing (DD) technique.

### **2.2.7 Integer Ambiguity and Cycle Slip**

The integer ambiguity represents the number of whole wavelengths in the phase difference at two antennas. It is not directly measurable. There is one integer ambiguity for each satellite per baseline. In other words, if three satellites are being tracked using three antennas (and two baselines) there will be six integer ambiguities to be determined. Once an integer ambiguity has been determined, it is maintained as long as the tracking loop maintains lock on the satellite signal; a cycle slip occurs if the tracking loop loses lock on the GPS signal. If undetected, a cycle slip causes the previously calculated integer ambiguity to be invalid. An incorrect integer ambiguity causes

a bias-type error in the attitude measurement. Because of its quantized nature, the integer ambiguity cannot be estimated in a linear Kalman filter. Search algorithms have been developed which exhaustively check the possibilities with varying degrees of efficiency. These algorithms usually require extensive computation, the use of extra satellites, and/or special receiver characteristics [7, 10]. At least one commercial manufacturer uses baselines shorter than the L1 wavelength ( $\lambda = 19$  cm) which eliminates the ambiguity [5]; but accuracy of this configuration is limited by the extremely short baseline. For high accuracy applications, a better solution is to couple the interferometer with a gyroscopic attitude reference system. When an attitude estimate is provided by gyroscopes, the integer ambiguity may be instantaneously determined, or highly constrained, depending on the accuracy of the estimate.

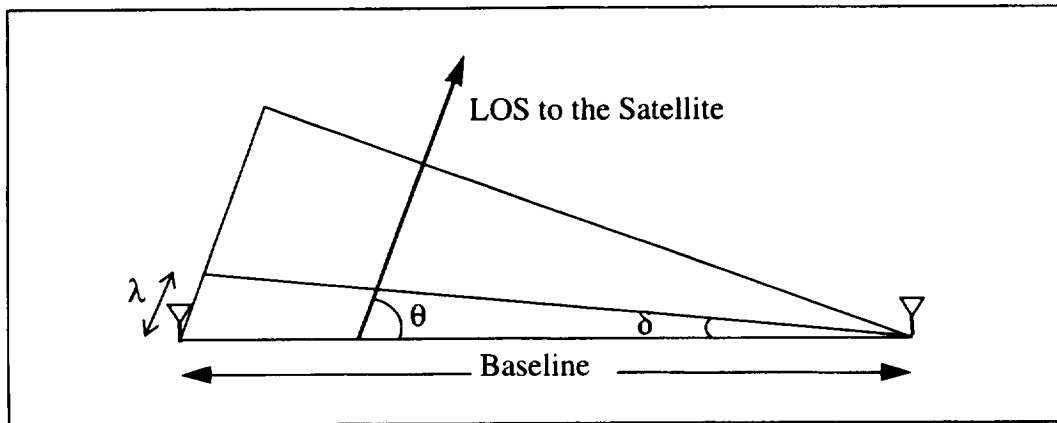


**Figure 2.4 Angular Effect of the Integer Ambiguity**

For example, consider a simple case where  $n=0$  or  $n=1$  (illustrated in Figure 2.4).  $\delta/2$  is the angular resolution required to resolve the integer ambiguity. It depends on the baseline length,  $b$ , and the direction to the satellite,  $\theta$ . For all values of  $\theta$ ,  $\delta$  and  $b$  are related by

$$\delta \leq \text{atan} \left( \frac{\lambda}{b} \right) \quad (2.1)$$

For baselines of 1 meter, an attitude estimate accurate to  $\pm 5^\circ$  is sufficient to uniquely determine the integer ambiguity. Then the integer ambiguity may be calculated at each measurement, rather than being a stored value. In this case, cycle slips would not occur. Alternately, since inertial systems are very reliable for short periods during high dynamics, they may be used both to detect the initial cycle slip, and to maintain an attitude measurement until GPS signal lock can be regained.

## 2.2.8 Satellite Geometry

Poor satellite geometry can degrade the accuracy of the GPS attitude measurement just as it degrades position and velocity measurements. However, the satellite geometry requirements are slightly different for attitude determination. As in the positioning problem, it is desirable that the satellites be spread out on the sky; but in addition the line of sight (LOS) to each satellite should be as perpendicular as possible to each baseline. When the satellites are not spread out, there tends to be a bias in the attitude solution [5, 12] (just as there would be for the position solution). As stated in Equation 1.2, the value of  $\cos\theta$  is calculated for the solution. Because the slope of  $\cos\theta$  is steepest around  $\theta = 90^\circ$ , the best angular resolution of  $\theta$  is obtained in that region. If double differences are used, the difference of the LOS vectors should be perpendicular to the baselines. The most precise measurements can be obtained if the satellite selection routine is applied separately for each baseline, rather than for the array as a whole [5]. In this case, different satellites may be selected for each baseline, increasing the number of receiver channels required and the complexity of the processing software.

At this point, no instantaneous figure of merit for attitude determination has been reported in the literature. Later in this thesis, a definition of ADOP will be presented, along with further discussion of the merits of various satellite selection routines.

## 2.3 Gyroscope Errors

The following describes the major error sources for ring laser gyros (RLGs), the type under consideration in this thesis.

### 2.3.1 Bias

All gyros are subject to bias drift rate, which causes a drift in the attitude solution over time. When the gyroscopes are coupled with a GPS interferometer, GPS measurements are available about once a second. Therefore, as long as unacceptable drift does not occur between measurements, a very large bias can be tolerated. In addition, nearly all of the bias is typically a random constant, which can easily be estimated in a Kalman filter if precise measurements are available.

### 2.3.2 Scale Factor Error

The angular output of a gyroscope varies proportionally to the angular input. However, the constant of proportionality is not known precisely, causing the slope of the output vs. input line to differ from the design slope, as shown in Figure 2.5. The difference between the true slope and the design slope is the scale factor error.

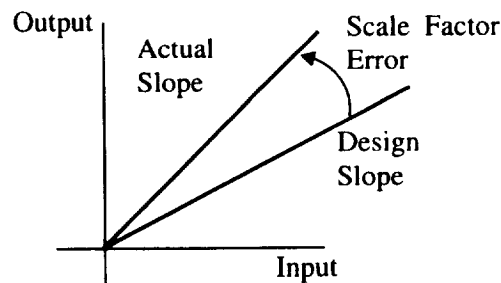


**Figure 2.5 Scale Factor Error**

### 2.3.3 Misalignment

The gyro misalignments are also called “non-orthogonalities.” Because of manufacturing limitations, the three single-degree-of-freedom gyroscopes required for an

attitude reference system cannot be mounted perfectly orthogonal, resulting in the misalignments. There are two misalignments for each gyro; for example, the x-axis gyro has one misalignment about the y-axis, and another about the z-axis. Therefore, there are a total of six misalignments. The misalignments may also be estimated, provided that the vehicle performs maneuvers which make the misalignments observable, and GPS or other reference measurements are available.

### **2.3.4 Angle Random Walk**

Noise on the angular rate output causes the attitude solution to wander or “random walk.” The filtering process can estimate part of the resulting attitude error, but cannot, of course, predict how the error will random walk. Therefore, angle random walk will directly limit the length of time that gyroscope accuracy can be maintained without GPS measurements or other alignments.

## **2.4 GPS Error Models**

Statistical error models are used to capture the effects of the errors in the linear covariance analysis. The phase error, including receiver noise, is modeled as zero mean white noise. The baseline flexures and path delays are both modeled as zero mean band-limited noise. Physically, that means that the baselines cannot flex with infinite frequency. It also means that the flexures are temporally correlated. The same is true of the electrical path length changes which cause the path delays.

This type of random process is adequately approximated by an exponentially correlated random variable (ECRV) [19], and has the autocorrelation function

$$\varphi_{xx}(\tau) = \sigma^2 e^{-\frac{|\tau|}{T}} \quad (2.2)$$

where  $\tau$  is the time difference variable, and  $T$  is the time constant. In the remainder of this thesis,  $\tau$  is used to denote the time constant of an ECRV. The time constant for both the baseline flexures and the path delays is tied to the heating and cooling which is caused by the vehicle moving in and out of the sunlight.

Multipath errors are also modeled as ECRVs [17, 20]; the multipath time constant is the time it takes for the LOS to the satellite to “significantly” change direction, or move through about  $30^\circ$  [25]. The multipath error on a measurement depends on the direction to the satellite; since the satellites are selected to be spread out in the sky, the multipath error from each satellite is modeled as independent. The multipath error from one satellite to each of the orthogonal baselines may be independent or highly correlated, depending on the local reflective environment. Thus the total multipath on a particular measurement,  $\xi_t$ , is modeled as

$$\xi_t = \xi_c + \xi_i \quad (2.3)$$

where  $\xi_c$  is the common multipath error, and  $\xi_i$  is the multipath error which is independent, or different between the two baselines.

Propagation errors and satellite clock errors are considered negligible (as discussed in the previous chapter), and ignored. It is assumed that a batch processing solution resolves the initial integer ambiguity (at system start-up) [10]. Once an attitude estimate exists, integer ambiguity can be calculated at each measurement using the gyroscopes, so that cycle slip is prevented. The interferometer/navigation base flexures were not modeled, but they may not be negligible. Any flexure of this type directly contributes to the attitude errors.

## **2.5 Gyroscope Error Models**

Gyroscope bias, scale factor, and misalignments are all modeled as random constants. Although long term instability does exist in each error source, it is not significant for the durations considered in this thesis.

Because the angular rate is integrated to produce attitude, the noise on the angular rate is also integrated. The effect of the noise is modeled as a random walk, which is valid to the extent that the noise is actually uncorrelated (white).



# Chapter 3

## Satellite Selection

### 3.1 Introduction

Poor satellite selection can contribute to the attitude measurement errors. Chapter 2 described in qualitative terms the recommended satellite geometry. In order to describe the satellite geometry quantitatively, it is necessary to define a numerical figure of merit. The literature discusses two possible ways to do this: AZDOP [13], and Pitch and Yaw Sensitivities (abbreviated PYS) [14]. AZDOP is a one dimensional figure of merit, i.e., it applies when only the heading is being measured. PYS is a two dimensional routine. While they provide useful information, both of these methods are inadequate for the three dimensional attitude problem presented here. This chapter presents the derivation of a three dimensional figure of merit, attitude dilution of precision (ADOP), for satellite selection. Sample calculations and geometries are described. An expanded, three dimensional version of Pitch and Yaw Sensitivities is also presented. GDOP was used in the simulation for comparison purposes, and is described in Appendix A.

### 3.2 Attitude Dilution of Precision

The effect of satellite geometry on measurement error is often described using dilution of precision factors. For example, if each measurement in a set has a standard deviation given by  $\sigma_0$ , then the standard deviation of a parameter of interest,  $\sigma$ , will be related to  $\sigma_0$  by [16]

$$\sigma = \text{DOP} \cdot \sigma_0 \quad (3.1)$$

DOP factors provide convenient, instantaneous figures of merit for selecting satellites.

The derivation of the DOP factor for three dimensional attitude (ADOP) used in this analysis is similar to the derivation of GDOP described in Leick [16]. First, Leick's definition of the design matrix is applied to the attitude determination problem. This yields the design matrix

$$\begin{array}{c}
 \begin{array}{c} \text{Parameters} \\ \xrightarrow{\hspace{10em}} \end{array} \\
 \begin{array}{ccc} \text{Roll} & \text{Pitch} & \text{Yaw} \end{array} \\
 A = \begin{bmatrix} \frac{\partial}{\partial \text{roll}} \text{obs}_1 & \frac{\partial}{\partial \text{pitch}} \text{obs}_1 & \bullet \\ \frac{\partial}{\partial \text{roll}} \text{obs}_2 & \bullet & \bullet \\ \bullet & \bullet & \bullet \\ \text{(etc.)} & & \end{bmatrix} \begin{array}{c} \downarrow \\ \text{Observables} \end{array}
 \end{array}$$

The observables may either be single differences (SD) or double differences (DD). (The sensitivities which appear in the design matrix are derived in the following sections.) Then

$$(A^T A)^{-1} = \begin{bmatrix} \sigma_\phi^2 & \sigma_{\phi\theta} & \sigma_{\phi\psi} \\ \sigma_{\theta\phi} & \sigma_\theta^2 & \sigma_{\theta\psi} \\ \sigma_{\psi\phi} & \sigma_{\psi\theta} & \sigma_\psi^2 \end{bmatrix} \quad (3.2)$$

where  $\phi$ ,  $\theta$ , and  $\psi$  represent roll, pitch, and yaw. The off-diagonal terms represent the cross correlations, so, for example,  $\sigma_{\phi\theta}$  represents  $\rho_{\phi\theta} \sigma_\phi \sigma_\theta$ , where  $\rho_{\phi\theta}$  is the correlation coefficient between roll and pitch errors. Assuming that the measurement noises are uncorrelated, ADOP is related to the design matrix by

$$\text{ADOP} = \sqrt{\text{tr} (A^T A)^{-1}} \quad (3.3)$$

which means that

$$\text{ADOP} = \sqrt{\sigma_{\phi}^2 + \sigma_{\theta}^2 + \sigma_{\psi}^2} \quad (3.4)$$

If the measurement noises are correlated, then ADOP is related to the design matrix by

$$\text{ADOP} = \sqrt{\text{tr}(\mathbf{A}^T \mathbf{R}^{-1} \mathbf{A})^{-1}} \quad (3.5)$$

The positive definite weighting matrix,  $\mathbf{R}$ , which is related to the correlation of the measurement errors, has the form

$$\mathbf{R} = \begin{bmatrix} 2 & 1 & 1 \\ 1 & 2 & 1 \\ 1 & 1 & 2 \end{bmatrix} \quad (3.6)$$

given that the double differences are all related back to a single satellite. These double differences can be computed in alternate manners; but the corresponding form of  $\mathbf{R}$  changes such that ADOP does not depend on the double difference definition.

### 3.2.1 Variations and Extensions of ADOP

Just as PDOP is extended to GDOP by including time, it may be desirable to include other parameters in ADOP. In particular, in the SD case the path delays may be included. Baseline coordinates could also be included. The number of other parameters that are included is limited by the number of independent measurements available, and hence the number of satellites used, since  $\mathbf{A}^T \mathbf{A}$  must have full rank for an inverse to exist.

### 3.2.2 Single Difference Sensitivities

All sensitivities were derived from the single difference measurement equation, which (omitting measurement noise sources) is

$$\text{SD} = (\mathbf{u}_R^I)^T \mathbf{C}_B^I \mathbf{b}_i^B + \rho_i \quad (3.7)$$

In Equation (3.7) the superscripts I and B indicate a vector coordinatized in the earth centered inertial frame, and the vehicle body frame, respectively, and the subscript i indicates which baseline was used for the measurement. The path delay is represented by  $\rho$ , and  $C_B^I$  is the current body to inertial transformation matrix.

The first step in the derivation is to express  $C_B^I$ , the vehicle attitude, in terms of the parameters of interest: roll,  $\phi$ , pitch,  $\theta$ , and yaw,  $\psi$ . Roll, pitch, and yaw are defined to be ordered, fixed-axis rotations. Therefore,  $C_B^I$  is related to  $\phi$ ,  $\theta$ , and  $\psi$  by

$$C_B^I = R_z(\psi)R_y(\theta)R_x(\phi) = \begin{bmatrix} c\psi & -s\psi & 0 \\ s\psi & c\psi & 0 \\ 0 & 0 & 1 \end{bmatrix} \begin{bmatrix} c\theta & 0 & s\theta \\ 0 & 1 & 0 \\ -s\theta & 0 & c\theta \end{bmatrix} \begin{bmatrix} 1 & 0 & 0 \\ 0 & c\phi & -s\phi \\ 0 & s\phi & c\phi \end{bmatrix}$$

where  $c\psi$  means  $\cos\psi$ ,  $s\theta$  means  $\sin\theta$  and so forth. When  $C_B^I$  is expanded

$$C_B^I = \begin{bmatrix} c\psi \cdot c\theta & c\psi \cdot s\theta \cdot s\phi - s\psi \cdot c\phi & c\psi \cdot s\theta \cdot c\phi + s\psi \cdot s\phi \\ s\psi \cdot c\theta & s\psi \cdot s\theta \cdot s\phi + c\psi \cdot c\phi & s\psi \cdot s\theta \cdot c\phi - c\psi \cdot s\phi \\ -s\theta & c\theta \cdot s\phi & c\theta \cdot c\phi \end{bmatrix}$$

The baselines used in this thesis were  $(b_1^B)^T = [1 \ 0 \ 0]$  and  $(b_2^B)^T = [0 \ 1 \ 0]$ .

Expanding the single difference for the first baseline gives

$$\begin{aligned} SD &= [u_x \ u_y \ u_z] C_B^I \begin{bmatrix} 1 \\ 0 \\ 0 \end{bmatrix} + \rho_1 \\ &= u_x \cdot c\psi \cdot c\theta + u_y \cdot s\psi \cdot c\theta - u_z \cdot s\theta + \rho_1 \end{aligned} \tag{3.8}$$

Then the sensitivities for the measurements taken across baseline 1 can be determined by taking partial derivatives of Equation (3.8), so that

$$\begin{aligned}
\frac{\partial}{\partial \phi} SD &= 0 \\
\frac{\partial}{\partial \theta} SD &= -u_x \cdot c\psi \cdot s\theta - u_y \cdot s\psi \cdot s\theta - u_z \cdot c\theta \\
\frac{\partial}{\partial \psi} SD &= -u_x \cdot c\theta \cdot s\psi + u_y \cdot c\theta \cdot c\psi \\
\frac{\partial}{\partial \rho_1} SD &= 1 \\
\frac{\partial}{\partial \rho_2} SD &= 0
\end{aligned} \tag{3.9}$$

Likewise, the expansion of the SD for the second baseline yields

$$\begin{aligned}
SD &= [u_x \ u_y \ u_z] C_B^I \begin{bmatrix} 0 \\ 1 \\ 0 \end{bmatrix} + \rho_2 \\
&= -u_x \cdot s\psi \cdot c\phi + u_y \cdot c\psi \cdot c\phi + u_x \cdot c\psi \cdot s\theta \cdot s\phi \\
&\quad + u_y \cdot s\psi \cdot s\theta \cdot s\phi + u_z \cdot c\theta \cdot s\phi + \rho_2
\end{aligned} \tag{3.10}$$

and the corresponding sensitivities are

$$\begin{aligned}
\frac{\partial}{\partial \phi} SD &= u_x \cdot s\psi \cdot s\phi - u_y \cdot c\psi \cdot s\phi + u_x \cdot c\psi \cdot s\theta \cdot c\phi + u_y \cdot s\psi \cdot s\theta \cdot c\phi \\
&\quad + u_z \cdot c\theta \cdot c\phi \\
\frac{\partial}{\partial \theta} SD &= u_x \cdot c\psi \cdot s\phi \cdot c\theta + u_y \cdot s\psi \cdot s\phi \cdot c\theta - u_z \cdot s\phi \cdot s\theta \\
\frac{\partial}{\partial \psi} SD &= -u_x \cdot c\phi \cdot c\psi - u_y \cdot c\phi \cdot s\psi - u_x \cdot s\theta \cdot s\phi \cdot s\psi + u_y \cdot s\theta \cdot s\phi \cdot c\psi \\
\frac{\partial}{\partial \rho_1} SD &= 0 \\
\frac{\partial}{\partial \rho_2} SD &= 1
\end{aligned} \tag{3.11}$$

### 3.2.3 Double Difference Sensitivities

In the DD case, the measurement equation (omitting measurement noise sources)

is

$$DD = (\underline{u}_{R1}^I - \underline{u}_{R2}^I)^T C_B^I \underline{b}_i^B \quad (3.12)$$

Thus, the sensitivities for the DD case can easily be obtained by substituting the difference of the LOS vectors,  $(\underline{u}_{R1} - \underline{u}_{R2})$ , for the LOS to a single satellite,  $\underline{u}_R$ , in the single difference equations. Therefore, the sensitivities for baseline 1 are

$$\begin{aligned} \frac{\partial}{\partial \phi} DD &= 0 \\ \frac{\partial}{\partial \theta} DD &= -(u_{x1} - u_{x2}) \cdot c\psi \cdot s\theta - (u_{y1} - u_{y2}) \cdot s\psi \cdot s\theta - (u_{z1} - u_{z2}) \cdot c\theta \\ \frac{\partial}{\partial \psi} DD &= -(u_{x1} - u_{x2}) \cdot c\theta \cdot s\psi + (u_{y1} - u_{y2}) \cdot c\theta \cdot c\psi \end{aligned} \quad (3.13)$$

and the sensitivities for baseline 2 are

$$\begin{aligned} \frac{\partial}{\partial \phi} DD &= (u_{x1} - u_{x2}) s\psi \cdot s\phi - (u_{y1} - u_{y2}) \cdot c\psi \cdot s\phi + (u_{x1} - u_{x2}) c\psi \cdot s\theta \cdot c\phi \\ &\quad + (u_{y1} - u_{y2}) \cdot s\psi \cdot s\theta \cdot c\phi + (u_{z1} - u_{z2}) \cdot c\theta \cdot c\phi \\ \frac{\partial}{\partial \theta} DD &= (u_{x1} - u_{x2}) \cdot c\psi \cdot s\phi \cdot c\theta + (u_{y1} - u_{y2}) \cdot s\psi \cdot s\phi \cdot c\theta \\ &\quad - (u_{z1} - u_{z2}) \cdot s\phi \cdot s\theta \\ \frac{\partial}{\partial \psi} DD &= -(u_{x1} - u_{x2}) c\phi \cdot c\psi - (u_{y1} - u_{y2}) c\phi \cdot s\psi - (u_{x1} - u_{x2}) s\theta \cdot s\phi \cdot s\psi \\ &\quad + (u_{y1} - u_{y2}) s\theta s\phi c\psi \end{aligned} \quad (3.14)$$

Since the path delays are not observable in the DD case, they are not included in ADOP.

### 3.2.4 Sample Calculations of ADOP

This section describes the calculation of ADOP for the satellite geometry shown in Figure 3.1, when single difference measurements are used. Subsequently, the position of satellite 3 is varied to show how ADOP changes with the changes in satellite geometry. The path delays are not included in these calculations.

For the sample calculations, it is assumed that the body coordinate frame is aligned

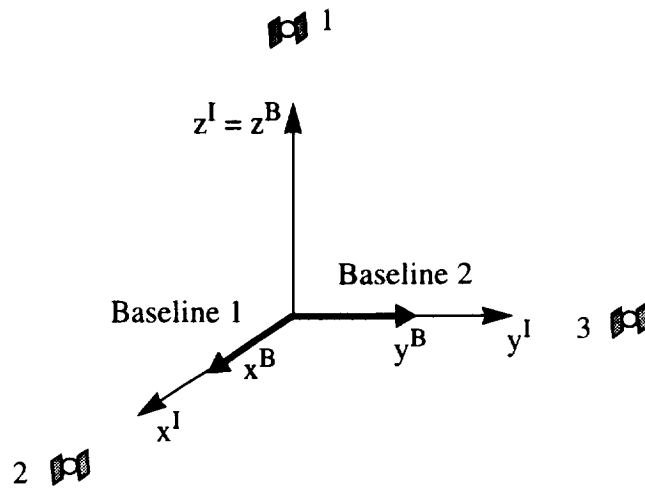


**Figure 3.1 Satellite Geometry**

with the inertial frame, so that

$$\phi = \theta = \psi = 0 \quad (3.15)$$

The unit LOS vectors for the satellite geometry shown are

$$\mathbf{u}_{R1}^T = [0 \ 0 \ 1]$$

$$\mathbf{u}_{R2}^T = [1 \ 0 \ 0]$$

$$\mathbf{u}_{R3}^T = [0 \ 1 \ 0]$$

Using Equations (3.9) and (3.11) to calculate the sensitivities,

$$\mathbf{A} = \begin{bmatrix} 0 & -1 & 0 \\ 1 & 0 & 0 \\ 0 & 0 & 0 \\ 0 & 0 & -1 \\ 0 & 0 & 1 \\ 0 & 0 & 0 \end{bmatrix} \quad (3.16)$$

The first two rows of  $A$  are the sensitivities of the single difference using satellite 1 and baselines 1 and 2, respectively. Equation (3.16) shows that measurements taken from the satellite overhead are sensitive to either roll or pitch, depending on which baseline is used. Measurements from either of the satellites on the horizon are sensitive to yaw only. Then

$$(A^T A)^{-1} = \begin{bmatrix} 1.0 & 0.0 & 0.0 \\ 0.0 & 1.0 & 0.0 \\ 0.0 & 0.0 & 0.5 \end{bmatrix}$$

and for this satellite geometry

$$ADOP = \sqrt{(A^T A)^{-1}} = 1.58$$

Because the baselines are orthogonal, ADOP does not vary when the azimuth of satellite 3 changes. Figure 3.2 shows how ADOP varies with the elevation of satellite 3.

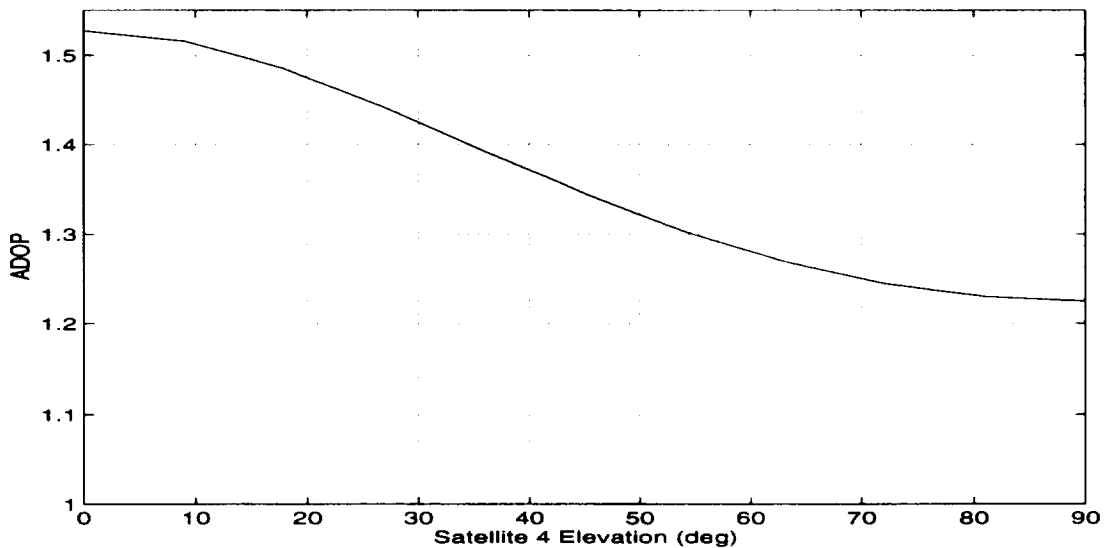


**Figure 3.2 ADOP Changes With Satellite Geometry**



### 3.3 Pitch and Yaw Sensitivities

This algorithm is based on a two dimensional algorithm presented previously [14]. That algorithm included equations for the elevation and azimuth sensitivities of a baseline which was nearly aligned with a local level frame, such that the antennas were always pointed away from the earth. Those equations have been adapted for space applications, where the orientation of the antenna array is completely arbitrary, and renamed the pitch and yaw sensitivities. The derivation of the equations used in this thesis from those presented in the reference is shown in Appendix B.

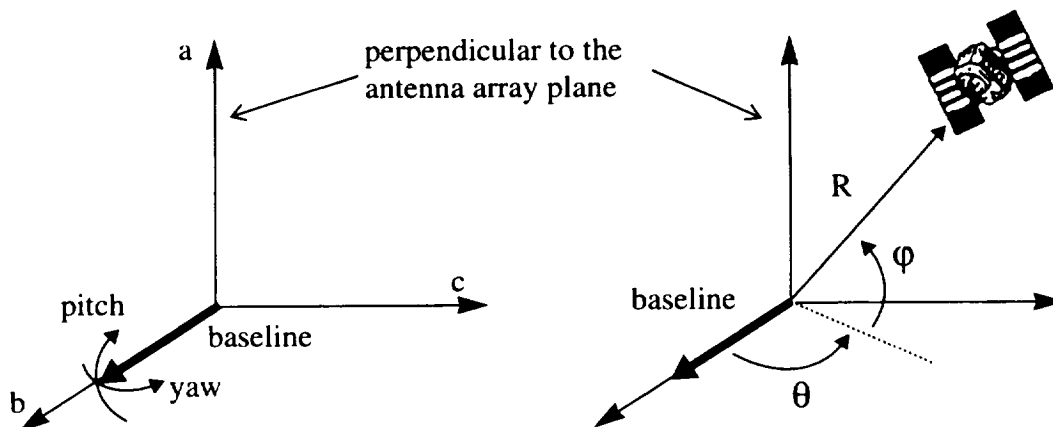


**Figure 3.3 Pitch and Yaw Sensitivities**

In the context of this algorithm, “pitch” and “yaw” refer to baseline movement about a nominal position, rather than spacecraft attitude. In Figure 3.3, pitch is rotation *out* of the antenna array plane, or about the *c*-axis, while yaw is rotation *in* the antenna array plane, about the *a*-axis.

“Pitch sensitivity” is the sensitivity of a particular SD or DD to baseline orientation in the pitch direction. “Yaw sensitivity” is the sensitivity to baseline orientation in the yaw direction. Both sensitivities are defined in terms of the spherical coordinates of the satellite with respect to the baseline in question:

$$PS = \sin\varphi \quad (3.17)$$

$$YS = \cos\varphi\sin\theta \quad (3.18)$$

If DD measurements are used, then the spherical coordinates of the difference of the LOS vectors, rather than the LOS to an individual satellite, are used when computing the sensitivities.

The pitch or yaw sensitivity of a group of four satellites (or three double differences) is calculated by taking the sum-squared of the individual sensitivities. Thus, each group has two total sensitivities, rather than a single figure of merit. Groups are rated against one another by comparing the minimum (or worst) sensitivities; the group with the largest (best) minimum sensitivity is ranked the highest.

# Chapter 4

## Linear Covariance Analysis

A linear covariance analysis computes the error statistics of a system. Therefore, it can be used as a tool used to predict system performance. This chapter begins with an overview of linear covariance analysis. Then, the simulation used for this thesis is described, and a flow chart is presented. Finally, the equations used to implement the linear covariance analysis in this simulation are described.

### 4.1 Overview

The linear covariance analysis is based on assumptions that the dynamics of the system are linear or can be linearized, that an estimate of the system state is maintained, that the errors in that estimate can be statistically described, and that these second-order statistics can be propagated in time.

The dynamics of the system state are described by

$$\dot{\underline{x}} = F\underline{x} + \underline{w} \quad (4.1)$$

where  $\underline{x}$  is the state vector,  $F$  is the dynamics matrix, and  $\underline{w}$  is Gaussian white noise. The analysis in this thesis focuses on the system state at discrete points in time,  $t_k$ ,  $t_{k+1}$ , ...; in that case the discrete dynamics can be described by a difference equation [8],

$$\underline{x}(t_{k+1}) = \Phi(t_{k+1}, t_k)\underline{x}(t_k) + \underline{w}_k \quad (4.2)$$

where  $\Phi(t_{k+1}, t_k)$  is the state transition matrix for the time step from  $t_k$  to  $t_{k+1}$ , and  $\underline{w}_k$  is the discretized noise.  $\underline{w}_k$  is related to  $\underline{w}$  by

$$\underline{w}_k = \int_{t_k}^{t_{k+1}} \Phi(t_{k+1}, \tau) \underline{w}(\tau) d\tau \quad (4.3)$$

While the actual value of the system state is not known, an estimate, denoted by  $\hat{x}$ , is maintained. The errors in the estimate, called the state errors, are defined as

$$\delta x_k = \hat{x}_k - x_k \quad (4.4)$$

These errors are described by their second-order statistics which together are called the covariance matrix, E. The covariance of the state errors is defined as

$$E_k = \langle \delta x_k \cdot \delta x_k^T \rangle \quad (4.5)$$

where  $\langle \rangle$  denotes the expectation operation.

If the initial value of E is known, then the knowledge of the state dynamics and any measurements that are performed can be used to calculate future values of E, or in other words, to provide a covariance analysis. The covariance analysis has two basic parts: (1) the process propagation, and (2) the measurements. The process is how the errors change due to the state dynamics alone. When the covariance matrix is known at time  $t_k$ , then it can be propagated to a future time  $t_{k+1}$  using [8]

$$E(t_{k+1}) = \Phi(t_{k+1}, t_k) E(t_k) \Phi^T(t_{k+1}, t_k) + Q_k \quad (4.6)$$

where  $Q_k$  is the discrete process noise matrix, and is also called the noise covariance matrix.  $Q_k$  is related to the process noise spectral density matrix, Q, by

$$Q_k = \int_{t_k}^{t_{k+1}} \Phi(t_{k+1}, \tau) Q(\tau) \Phi^T(t_{k+1}, \tau) d\tau \quad (4.7)$$

and to the discretized noise by

$$Q_k = \langle \underline{w}_k \cdot \underline{w}_k^T \rangle \quad (4.8)$$

The process propagation evolves the covariance matrix to the times at which the measurements occur.

The second major part of the linear covariance analysis is the measurement incorporation. Measurements are taken in order to reduce the state errors. It is assumed that each group of simultaneous measurements,  $\underline{z}$ , can be modeled as a linear combination of the state plus some Gaussian noise. The relationship between the measurements and the state is given by

$$\underline{z}_k = \mathbf{H}_k \underline{x}_k + \underline{v}_k \quad (4.9)$$

The observation matrix,  $\mathbf{H}_k$ , and the measurement noise,  $\underline{v}_k$ , as well the method used to incorporate the new measurement with the previous estimate, determine the effect of a particular measurement on the error covariance matrix. Although there are many approaches to incorporating measurements, the one which is most common is the Kalman filter equation. If the state estimate is updated in this manner, then the new covariance matrix is related to the old by [8]

$$\mathbf{E}^+ = \mathbf{E}^- - \mathbf{E}^- \mathbf{H}_k^T (\mathbf{H}_k \mathbf{E}^- \mathbf{H}_k^T + \mathbf{R}_k)^{-1} \mathbf{H}_k \mathbf{E}^- \quad (4.10)$$

where the measurement noise matrix,  $\mathbf{R}$ , is defined as:

$$\mathbf{R}_k = \langle \underline{v}_k \cdot \underline{v}_k^T \rangle \quad (4.11)$$

$\mathbf{E}^-$  and  $\mathbf{E}^+$  are used to designate the covariance matrix before and after the measurement has been incorporated, respectively.

If the measurement errors,  $\underline{v}_k$ , are not correlated with each other, then  $\mathbf{R}_k$  will have the diagonal form

$$\mathbf{R}_k = \begin{bmatrix} \langle v_1 v_1 \rangle & \langle v_1 v_2 \rangle & \langle v_1 v_3 \rangle & \dots \\ \langle v_2 v_1 \rangle & \langle v_2 v_2 \rangle & \langle v_2 v_3 \rangle & \dots \\ \langle v_3 v_1 \rangle & \langle v_3 v_2 \rangle & \langle v_3 v_3 \rangle & \dots \\ \dots & \dots & \dots & \dots \end{bmatrix} = \begin{bmatrix} \alpha_1^2 & 0 & 0 & \dots \\ 0 & \alpha_2^2 & 0 & \\ 0 & 0 & \alpha_3^2 & \\ \dots & & & \dots \end{bmatrix} \quad (4.12)$$

Then the measurements can be incorporated sequentially, rather than in a batch. In this case, each individual measurement is modeled as

$$z_k = \mathbf{h}_k^T \mathbf{x}_k + v_k \quad (4.13)$$

where  $\mathbf{h}_k$  is the sensitivity vector,  $v_k$  is the measurement noise, and  $\langle v_k^2 \rangle = \alpha_k^2$ . Each measurement can then be incorporated using

$$\mathbf{E}^+ = \mathbf{E}^- - \mathbf{E}^- \mathbf{h}_k (\mathbf{h}_k^T \mathbf{E}^- \mathbf{h}_k + \alpha_k^2)^{-1} \mathbf{h}_k^T \mathbf{E}^- \quad (4.14)$$

Sequential incorporation is sometimes preferred, because the measurements do not have to be taken at exactly the same time, and it is possible to incorporate some of the measurements, even if others are not available. There is also a computational advantage, in that there is no need to take a matrix inverse in Equation (4.14).

## 4.2 Simulation

The linear covariance analysis developed for this thesis includes a simulation of a spacecraft in low earth orbit. Orbital conditions typical for a shuttle or station type spacecraft were chosen. Attitude estimates are provided by a gyroscopic attitude reference system, which are updated with GPS carrier phase difference measurements. A flow chart for the simulation used for this thesis is shown in Figure 4.1.

Also included is a simulation of the GPS constellation, which approximates the satellites' orbits as circular, with an altitude of approximately 26,600 km. The modelled constellation contains 24 satellites, arranged in 6 rings of 4 satellites each. The

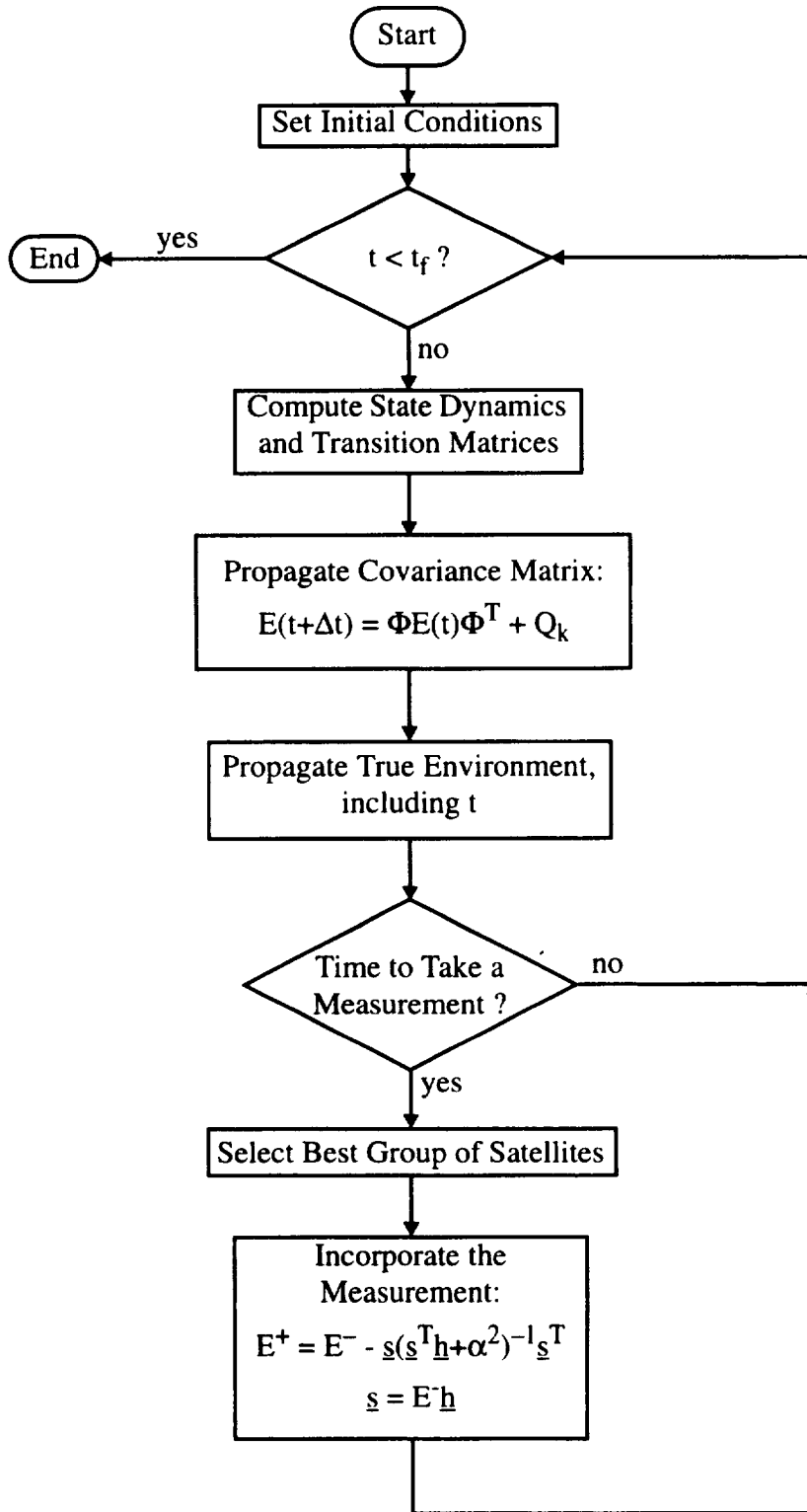


Figure 4.1 Simulation Flow Chart

rings are equally spaced in argument of latitude, and at an inclination of 55°. Table 4.1 gives the details of the position of each satellite in its ring.

**Table 4.1 GPS Satellite Constellation**

Ring Number	Longitude of the Ascending Node (deg)	True Anomaly for Each Satellite in the Ring (deg)			
1	0.0	190.96	220.48	330.17	83.58
2	60.0	249.90	352.12	25.25	124.10
3	120.0	286.20	48.94	155.08	183.71
4	180.0	312.30	340.93	87.06	209.81
5	240.0	11.90	110.76	143.88	246.11
6	300.0	52.42	165.83	275.52	305.04

### 4.3 Implementation

In this section, the equations used to implement the linear covariance analysis are presented. Included are the equations for the error models discussed in Chapter 2, and the details of the covariance propagation. The complete error state vector for the SD case is  $\underline{x}^T = [ \psi^T \ \epsilon^T \ \beta^T \ \gamma^T \ \delta b_1^T \ \delta b_2^T \ \xi^T \ \rho_1^T \ \rho_2^T ]$ . Each element of the error state is described in Table 4.1. A more detailed description of each error was given in Chapter 2.

In the DD case, the path delays are not included in the state. The following sections describe the error state dynamics and the measurement incorporation.

#### 4.3.1 Process Dynamics

The state transition matrix is used to propagate the error state covariance matrix according to Equation (4.6). Since there is no closed form solution for the state transition matrix, it is calculated using the approximation [8]



**Table 4.2 Elements of The Error State Vector**

Symbol	Description	Number of Elements
$\Psi$	Attitude Error	3
$\epsilon$	Gyro Bias Error	3
$\beta$	Gyro Scale Factor Error	3
$\gamma$	Gyro Misalignment	6
$\delta b_1$	Baseline 1 Error	3
$\delta b_2$	Baseline 2 Error	3
$\xi$	Multipath Error	12
$\rho_1$	Path Delay 1	1
$\rho_2$	Path Delay 2	1

$$\Phi = I + F\Delta t + \frac{\Delta t^2}{2!} F^2 + \dots \text{ (H. O.T.)} \quad (4.15)$$

which is truncated at the second-order term. It is assumed that  $F$  is, or can be approximated as, constant over  $\Delta t$ . Sufficient accuracy is ensured by comparing the fourth term in the sequence with the  $\Phi$  approximated as the sum of the first three. A warning is printed if the ratio of any element in the fourth term to its corresponding element in the approximated  $\Phi$  exceeds one one-thousandth.

#### ***4.3.1.1 Attitude Errors and Gyroscope Dynamics***

The error in the attitude solution that is produced by the gyroscopes is determined by the various gyro errors: bias,  $\epsilon$ , scale factor,  $\beta$ , the misalignments,  $\gamma$ , and the white noise  $\eta$ , which produces angle random walk. The dynamics of the gyro process, coordinatized in the body frame are

$$\dot{\underline{\psi}}^B = (-\underline{\omega}_B^I \times \underline{\psi}^B) + \underline{\varepsilon}^B + \begin{bmatrix} \omega_x & 0 & 0 \\ 0 & \omega_y & 0 \\ 0 & 0 & \omega_z \end{bmatrix} \underline{\beta}^B + \begin{bmatrix} -\omega_z & \omega_y & 0 & 0 & 0 & 0 \\ 0 & 0 & \omega_z & -\omega_x & 0 & 0 \\ 0 & 0 & 0 & 0 & -\omega_y & \omega_x \end{bmatrix} \underline{\gamma}^B + \underline{\eta}^B \quad (4.16)$$

where  $\underline{\psi}^B$  is the attitude error vector,  $\underline{\omega}_B^I$  is the body rotation rate with respect to the inertial frame, and  $\omega_x$ ,  $\omega_y$ , and  $\omega_z$  are the components of  $\underline{\omega}_B^I$ . The first four terms of Equation (4.16) appear directly in the dynamics matrix. Since  $\eta$  is a noise term, it appears in the spectral density matrix,  $Q$ , rather than in the dynamics matrix. The complete dynamics and noise matrices are shown in Appendix C.

#### 4.3.1.2 Baseline Errors, Path Delays, and Multipath

Since each baseline coordinate error, each path delay, and the multipath error associated with each satellite is modeled as an ECRV, the dynamics of these errors are independent and have the same form. The dynamics for a general ECRV,  $x$ , are [8]

$$\dot{x} = -\frac{1}{\tau}x + v \quad (4.17)$$

where  $\tau$  is the time constant, and  $v$  is white noise. The discretized covariance of  $v$  over a time step  $\Delta t$  depends on the variance of the random process,  $\sigma_x^2$ , the time constant,  $\tau$ , and the time step,  $\Delta t$ . It is given by [8]

$$\sigma_x^2 \left( 1 - e^{-\frac{2\Delta t}{\tau}} \right) \quad (4.18)$$

The complete dynamics matrix and process noise matrix are shown in Appendix C.

#### 4.3.2 Measurement Updates

All measurements were incorporated sequentially, using Equation (4.14). As stated previously, two types of measurements are used, single differences (SD) and double differences (DD). Only one measurement type is used during a particular run.

#### ***4.3.2.1 Single Difference Measurements***

When SDs are used, the measurement noises are uncorrelated, and the measurements can be incorporated directly using the sequential form. The relationship between the sensitivity vector and the measurement is shown in Equation (4.13). The sensitivity vector can be calculated from Equation (3.7); the complete derivation is shown in Appendix D. The nonzero parts of the sensitivity vector are  $\underline{h}_\psi$  (attitude error),  $\underline{h}_{b1}$  or  $\underline{h}_{b2}$  (baseline errors) depending on whether this measurement was taken using baseline 1 or baseline 2,  $\underline{h}_\xi$  (multipath), and  $h_{pd1}$  or  $h_{pd2}$  (path delays), again depending on the baseline in question.

The measurement noise term,  $\alpha^2$ , used to incorporate the measurement is simply  $\langle v^2 \rangle$ .

Care must be taken when updating the multipath states. Since each multipath error belongs to a certain satellite, when a change in the satellites used for measurement occurs, the variance for a new satellite's multipath must be reset to the initial value, and the appropriate cross-correlations must be set to zero.

#### ***4.3.2.2 Double Difference Measurements***

When DD are used, the measurement noises are correlated, and the measurements cannot be incorporated directly using the sequential form. However, the measurements can still be incorporated sequentially if they are first decorrelated. This is done by transforming the measurements so that the new measurement noise matrix has a diagonal form. The details of this process are shown in Appendix D. The measurement noise term,  $\alpha^2$ , for each measurement is taken from the diagonal of the new measurement noise matrix.

The non-zero parts of the sensitivity vector (before the decorrelating transformation) for the DD case are  $\underline{h}_\psi$  (attitude error),  $\underline{h}_{b1}$  or  $\underline{h}_{b2}$  (baseline errors) depending on

whether this measurement was taken using baseline 1 or baseline 2, and  $\underline{h}_\xi$  (multipath). As in the SD case, care must be used in regards to the multipath state.

# Chapter 5

## Results

The linear covariance simulation presented in the last chapter was used to analyze the performance of a GPS/inertial attitude determination system. This chapter summarizes the results of the simulation runs. A description of the factors which affect the system performance is presented, and a nominal run is defined. Finally, the results for various performance factors are presented and discussed.

### 5.1 Performance Factors and Nominal Conditions

The performance of a GPS/inertial attitude determination system is affected by many factors. In order to understand the effects of each performance factor, they must be varied individually. A nominal run was defined which served as the baseline for these variations. The factors which were varied in this thesis, along with the range of values which were considered, are discussed in the following section. Subsequently, the nominal run conditions are described, including those factors which were not varied in this thesis.

#### 5.1.1 Performance Factors

The performance factors which were varied, along with the range of values considered, are listed in Table 5.1. The phase error listed is the error on a single phase measurement. A phase error of  $3^\circ$  is equivalent to a 1.6 mm error in the range to the satellite. The multipath correlation refers to the correlation between the multipath from one satellite to each of the two baselines. The good quality gyro was selected to have characteristics similar to those of the ring laser gyroscope system proposed for the

Space Station; the poor quality gyro has significantly larger errors, such as a micromechanical gyroscope might have.

**Table 5.1 Performance Factors**

Performance Factor	Range of Values Considered	
Measurement Type	SD, DD	
Satellite Selection	SD: GDOP, PYS, ADOP, Extended ADOP DD: GDOP, PYS, ADOP	
Baseline Flexure Error	$\sigma = 0, 1, 5, 10$ mm	
Multipath Error Level	$\sigma = 0, 1.9, 3.8$ mm	
Multipath Correlation	0, 50, 100%	
Orbital Inclination	0°, 51.6°, 90°	
Attitude Hold	LVLH, Inertial, Maneuvers	
Gyroscope Quality	Good	Poor
Drift Bias (°/hr)	0.01	10.0
Scale Factor Error (ppm)	2.3	30.0
Misalignment (arcsec)	8.3	100.0
Angle Random Walk °/ $\sqrt{\text{hr}}$	0.0033	0.5

### 5.1.2 Nominal Run Conditions

Table 5.2 shows the conditions which were defined as the nominal run. The orbital altitude and eccentricity were chosen to be typical of a space station type vehicle. The same GPS constellation was used for all the runs, so that while the satellites visible to the spacecraft may have changed due to the orientation of the spacecraft, the GPS satellites were always in the same place at the same time in every run. In general, the selection of the GPS measurement rate depends on vehicle dynamics and performance requirements, as well as the capability of available equipment. For vehicles with low dynamics and long mission periods, such as the Space Station, which is considered in this thesis, the steady state accuracy is more pertinent than the short term response.

**Table 5.2 Nominal Run Conditions**

Factor	Condition or Value
Orbital Altitude	110 nm (204 km)
Orbital Eccentricity	0.0
GPS Constellation	As Described in Section 4.2
GPS Measurement Rate	1 Measurement Every 20 seconds
Baseline Configuration	2 Orthogonal Baselines: 1 Along the Body X-Axis, 1 Along the Body Y-Axis
Baseline Length	1 m
Phase Error	3°
Path Delays	$\sigma = 2 \text{ mm}, \tau = 2657 \text{ s}$
Baseline Flexure Error	$\sigma = 5 \text{ mm}, \tau = 2657 \text{ s}$
Multipath Error	$\sigma = 1.9 \text{ mm}, \tau \approx 770 \text{ s}$
Multipath Correlation	50%
Measurement Type	SD
Satellite Selection	Extended ADOP
Orbital Inclination	51.6°
Attitude Hold	LVLH
Gyroscope Quality	Good

The effect of the measurement rate on the performance was investigated by conducting several runs which differed from the nominal case only by the GPS measurement rate. The results of these runs are shown in Figure 5.1.

It can be seen from the figure that attitude error is estimated more quickly when a faster measurement rate is used. However, after about 5000 seconds, the attitude accuracy is nearly the same, regardless of the measurement rate. Based on these results, the frequency of GPS measurements was chosen to be only one every 20 seconds,

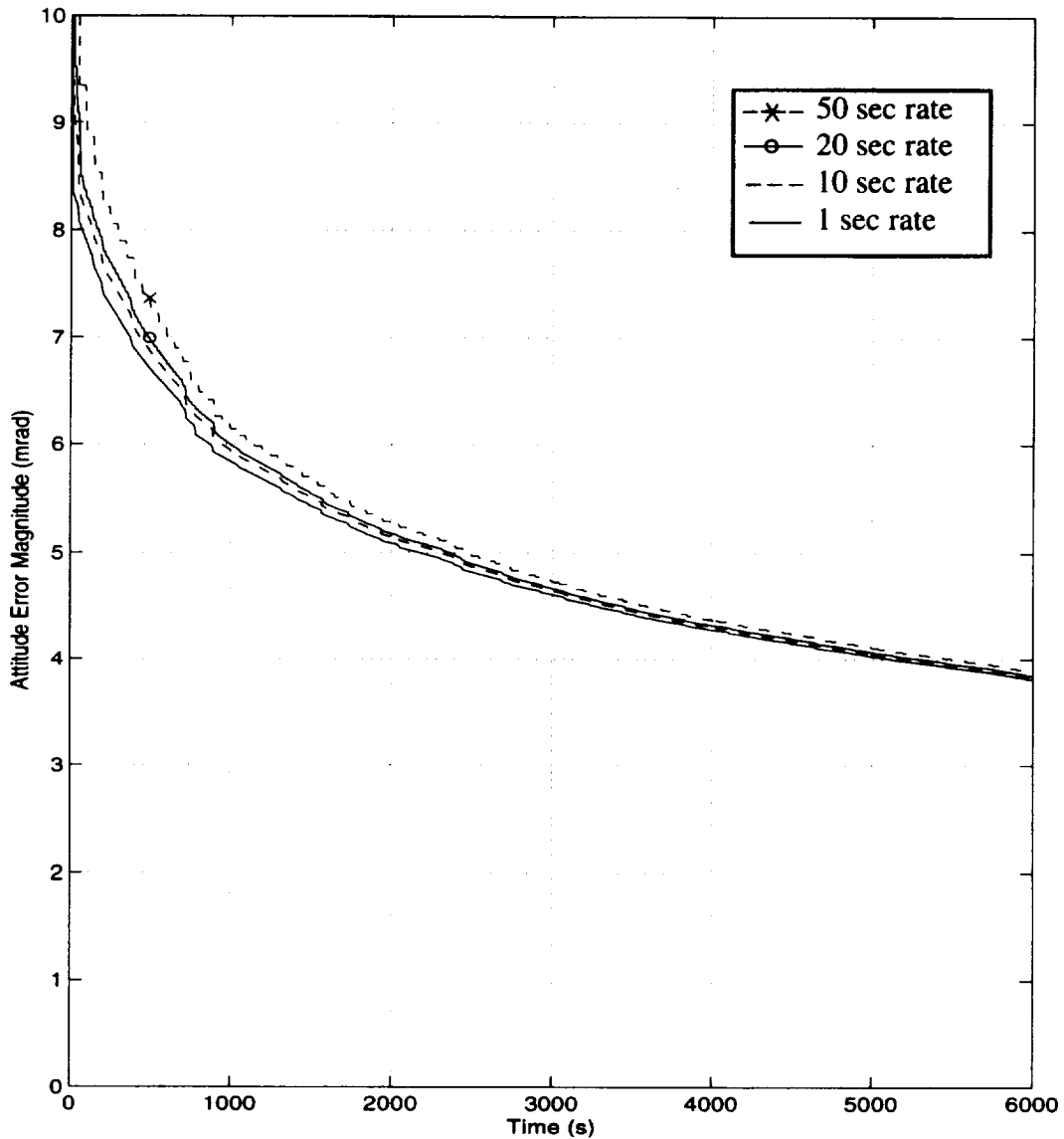


**Figure 5.1 Effect of GPS Measurement Rate on Attitude Errors**

although most currently available equipment is capable of producing measurements at about 1 Hz.

The time constants for both the baseline errors and the path delays are equivalent to one half of an orbital period. The time constant for each multipath ECRV depends on the rate of change of the LOS to the satellite; it computed dynamically in the simulation.



## 5.2 Results for the Nominal Run

This section describes the results for the nominal run in detail. Plots of the square root of every diagonal element of the state vector error covariance matrix are presented and discussed.

### 5.2.1 Attitude Error

Plots of each component of the attitude error, as well as the root sum square (RSS) of the components, are shown in Figure 5.2. All of the components of attitude error are substantially reduced by a single GPS measurement (see Table 5.3); however, the system has a long settling time, approximately 50,000 s, as indicated on the figure.

After the first measurement, the z-component of attitude error is smaller than the x- and y-components; this difference is due to the baseline configuration. Rotation about the body z-axis can be measured using both baselines, while rotation about the body x-axis can only be measured using the baseline 2 (which is along the body y-axis), and rotation about the body y-axis can only be measured using baseline1 (which is along the body x-axis). However, after about one orbit, the y-component of attitude error is much larger than the x- and z-components. This result is related to the nominal attitude hold orientation, in which the spacecraft is rotating about its body y-axis at the orbital

rate. This rotation apparently makes it more difficult to estimate the y-component of attitude error. This result will be further investigated in Section 5.3.6.

**Table 5.3 Attitude Errors for the Nominal Case**

Component	Attitude Error (mrad)			
	t = 0 seconds	t = 20 seconds	t = 6000 seconds	t = 86400 seconds
X	17.45	5.94	1.20	0.36
Y	17.45	5.97	3.45	1.89
Z	17.45	4.43	1.20	0.36
RSS	30.23	9.52	3.84	1.96

### 5.2.2 Baseline Errors

The errors in each component of each of the baselines are shown in Figure 5.3. The noisy appearance of the baseline errors is due to the fact that they were modeled as ECRV's. Other error sources create a noise floor, below which it is not possible to reduce any of the baseline errors.

The lengths of the baselines (the x-component of baseline 1, and the y-component of baseline 2) are estimated more quickly than the other components, because they are more easily distinguished from vehicle rotation. The z-component of baseline 1 is much more difficult to estimate than any of the other components. Since baseline 1 is along the x-axis, a z-component error is equivalent to a rotation about the y-axis, and it is difficult for the system to distinguish this baseline flexure from the vehicle rotation, which is also about the y-axis.

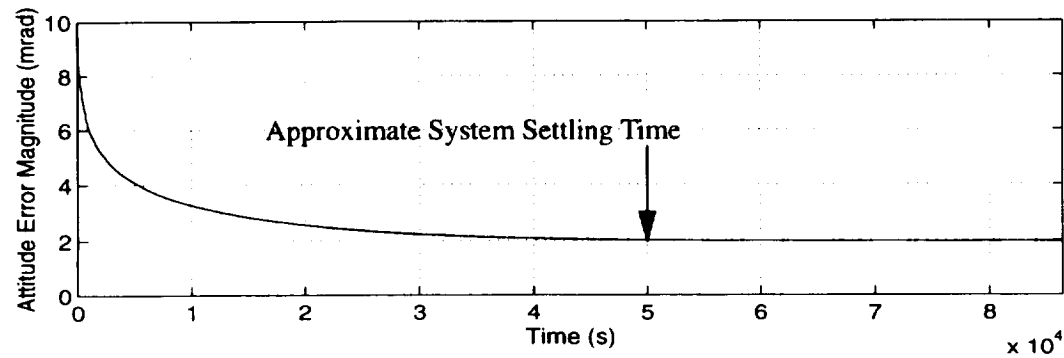
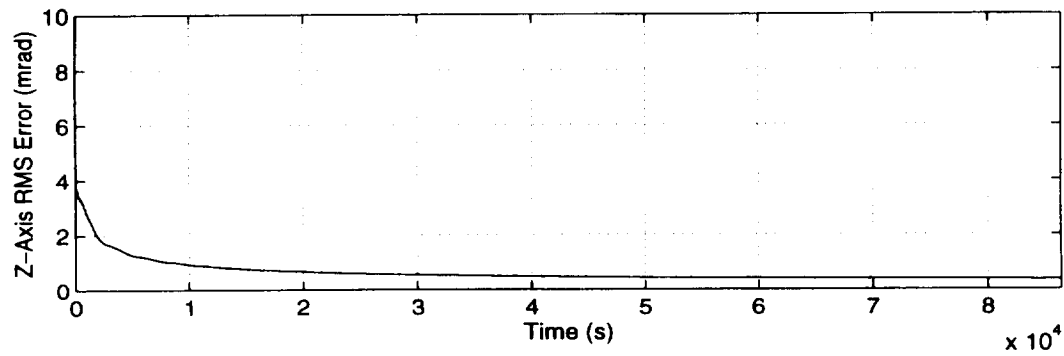
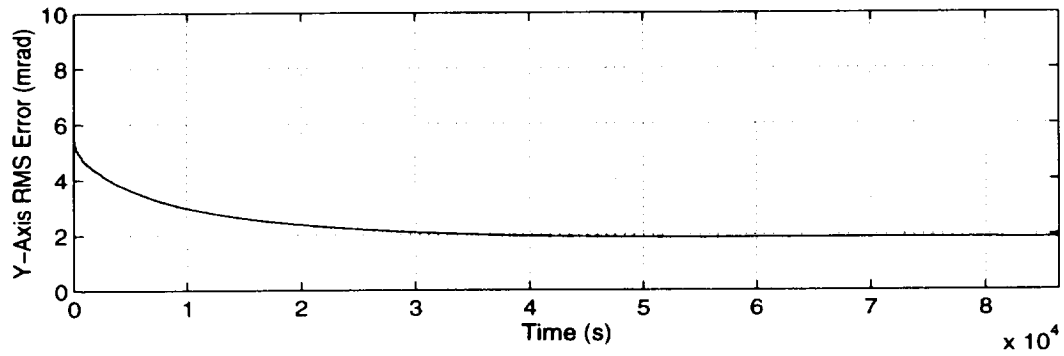
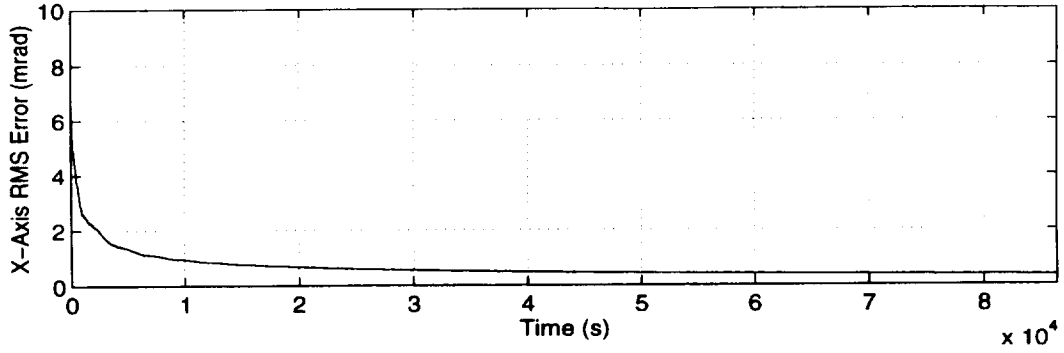


**Figure 5.2 Nominal Case Attitude Errors**

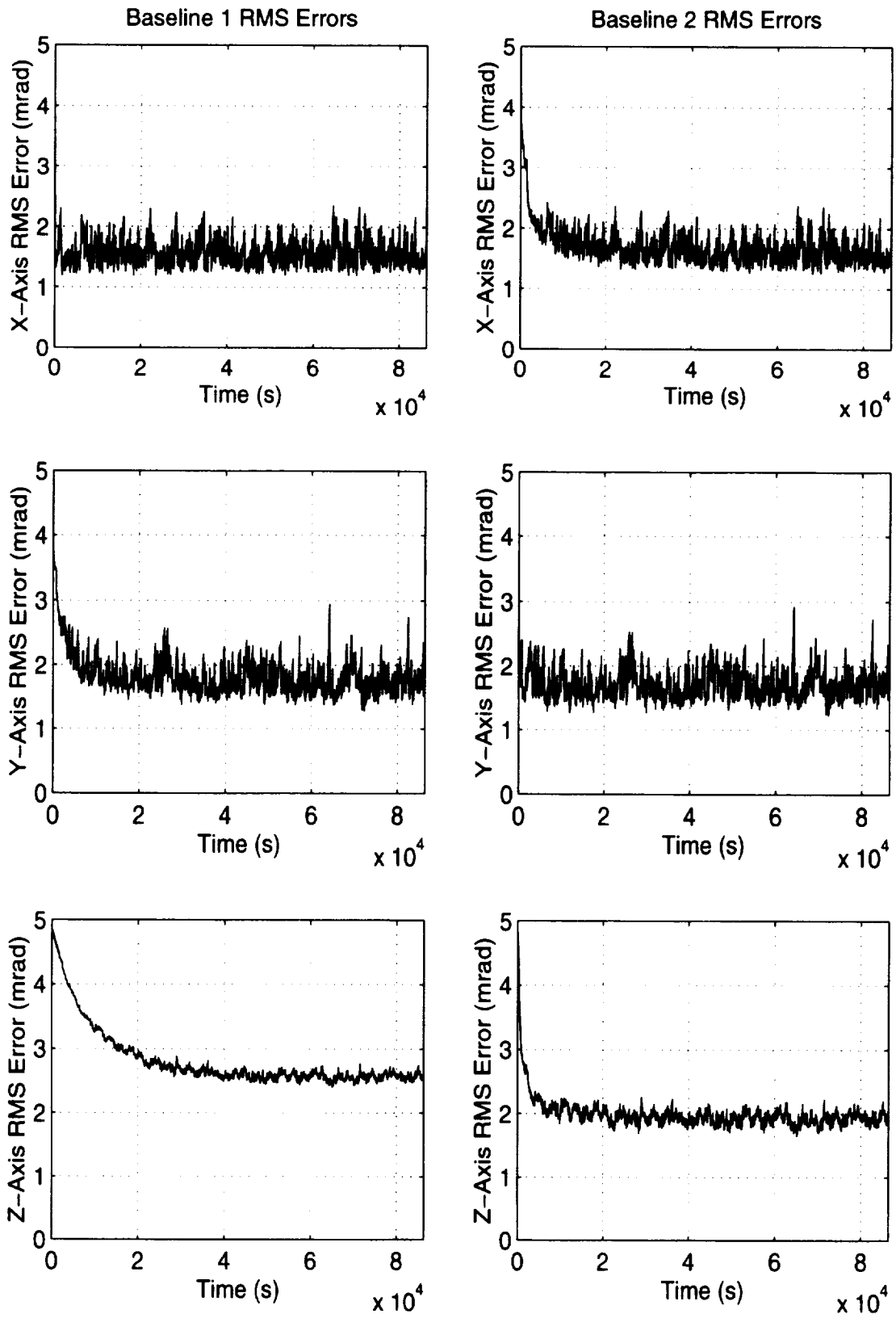


**Figure 5.3 Baseline Errors**

### 5.2.3 Multipath Errors

The total multipath error on a particular measurement was modeled as the combination of the multipath which is common to both baselines, and the multipath which is independent between the baselines. Thus, the variance of the total multipath error,  $\sigma_t^2$ , is related to the variances of these components by

$$\sigma_t^2 = \sigma_c^2 + \sigma_i^2 + 2\rho_{ci}\sigma_c\sigma_i \quad (5.1)$$

where  $\rho_{ci}$  is the correlation factor between the two multipath components.

The standard deviation for one of the multipath states for baseline 1 is shown in Figure 5.4. The other seven multipath states have very similar settling times and

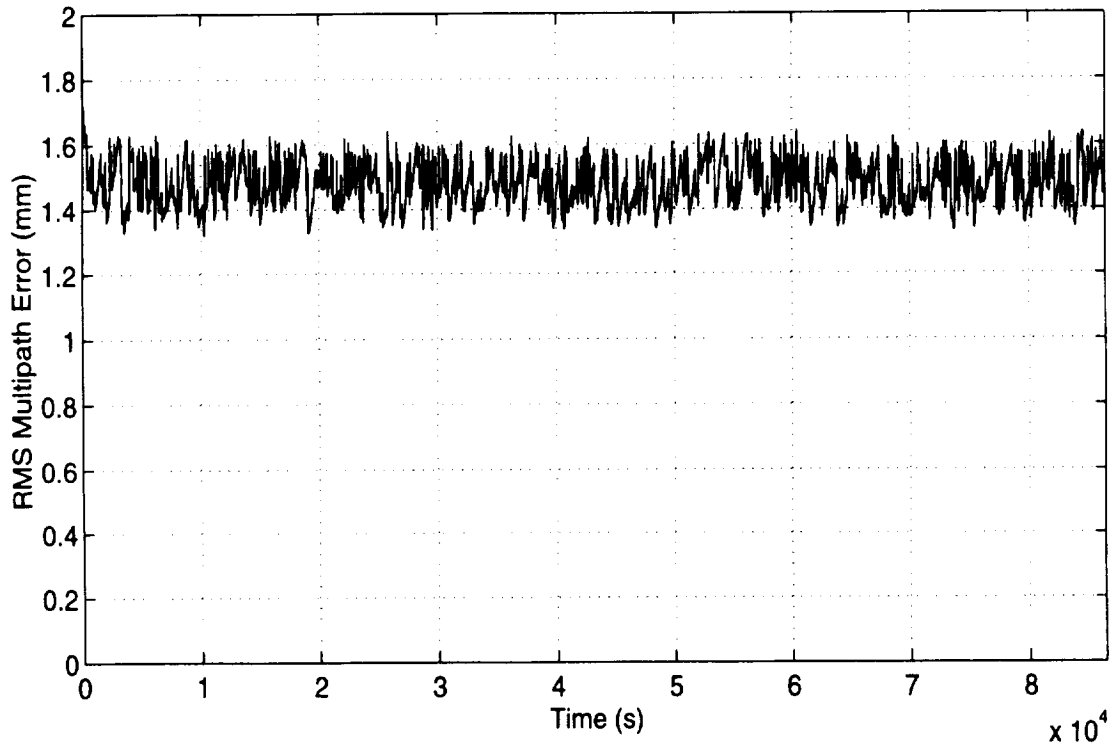


**Figure 5.4 Nominal Case Multipath Error**

steady state values. As with the baseline errors, the noisy appearance is a result of using an ECRV to model this error. There is a noise floor which prevents reduction of the multipath error below about 1.5 mm.

An expansion of the first 6000 seconds of Figure 5.4 is shown in Figure 5.5. The

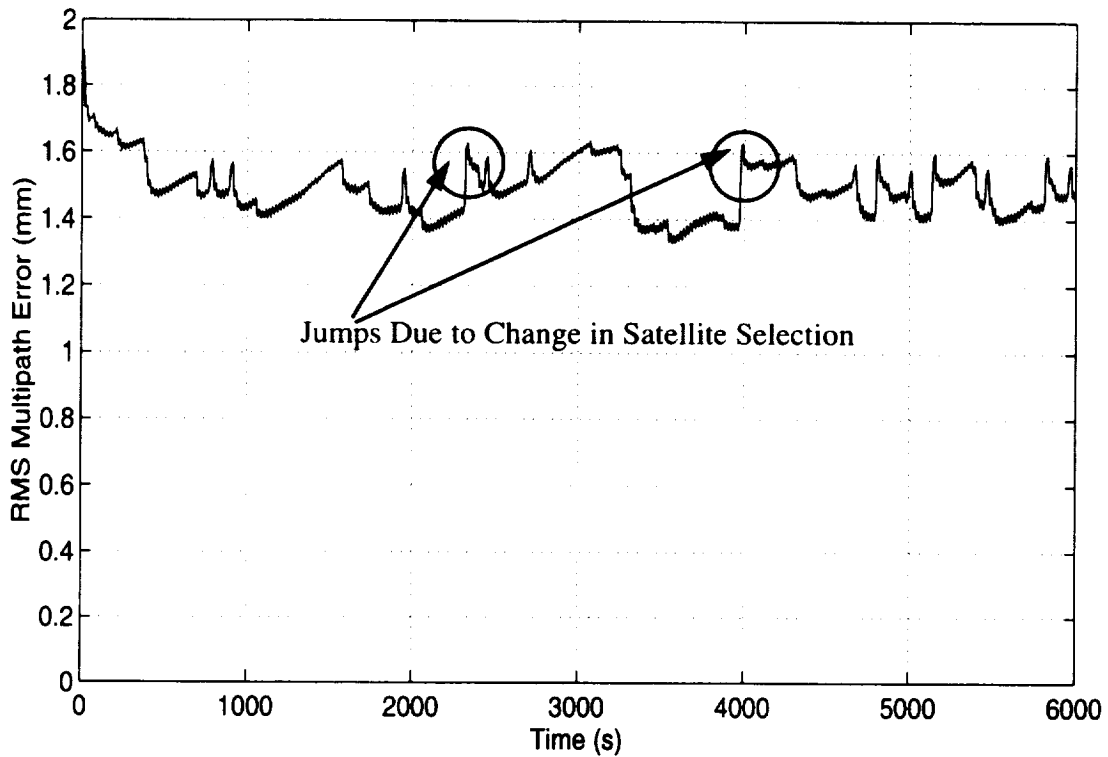


**Figure 5.5 Multipath Error**

sharp peaks which are indicated on the graph show when changes were made in the satellite selection. These peaks do not extend up to the initial error level because a measurement is incorporated immediately after the satellite change, and the post-measurement value is saved and plotted. The difference between the initial error and the level of the peaks indicates the amount of estimation that is possible with a single measurement. The frequent switching of satellites makes the estimation of the multipath error more difficult.

#### **5.2.4 Path Delays**

The path delays were only estimated when single difference measurements were used, since the delays are not observable using double difference measurements. Figure 5.6 shows the RMS magnitude of the path delay for baseline 1. As with the other

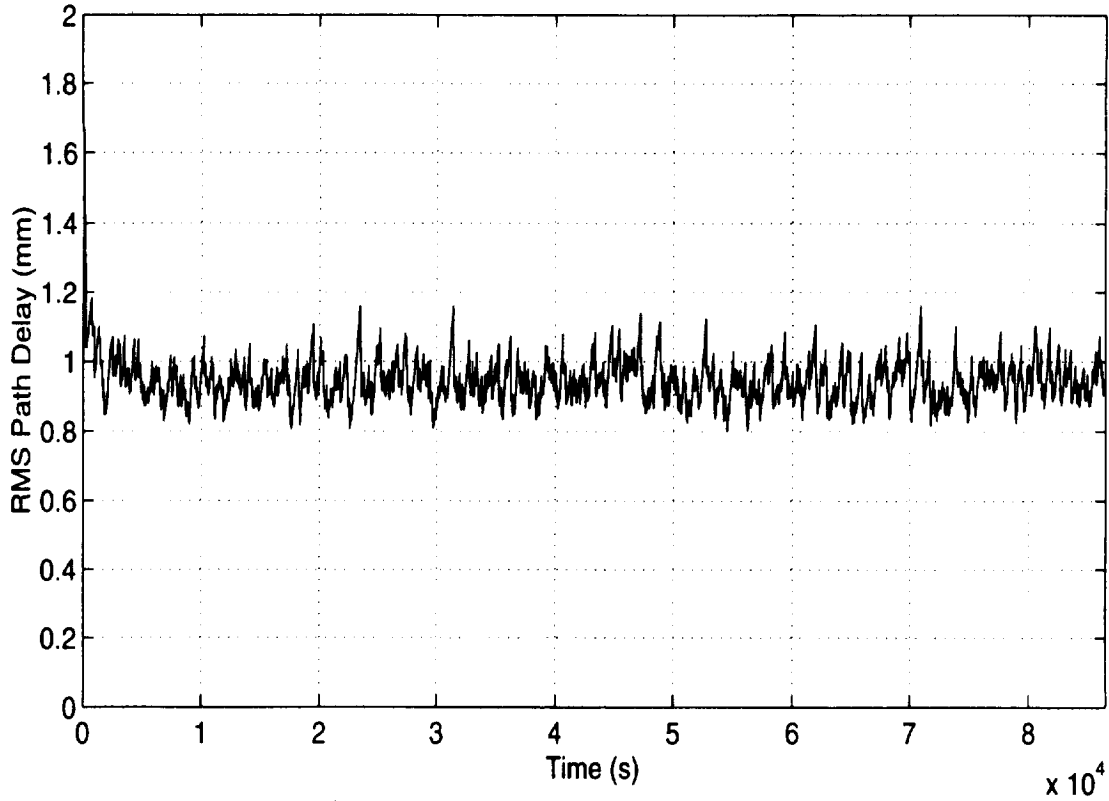


**Figure 5.6 Path Delay for Baseline 1**

errors which were modeled as ECRV's, the path delay is noisy in appearance. There is also a noise floor which limits the estimation of the path delay below about 1 mm.

### 5.2.5 Gyroscope Errors

None of the gyroscope errors are estimated very well, because they contribute only a small amount of error in the time between each measurement. Figure 5.7a, b, and c show the gyro bias, scale factor errors, and misalignments, respectively. Not every component of each error is observable in the nominal case, because the vehicle is only

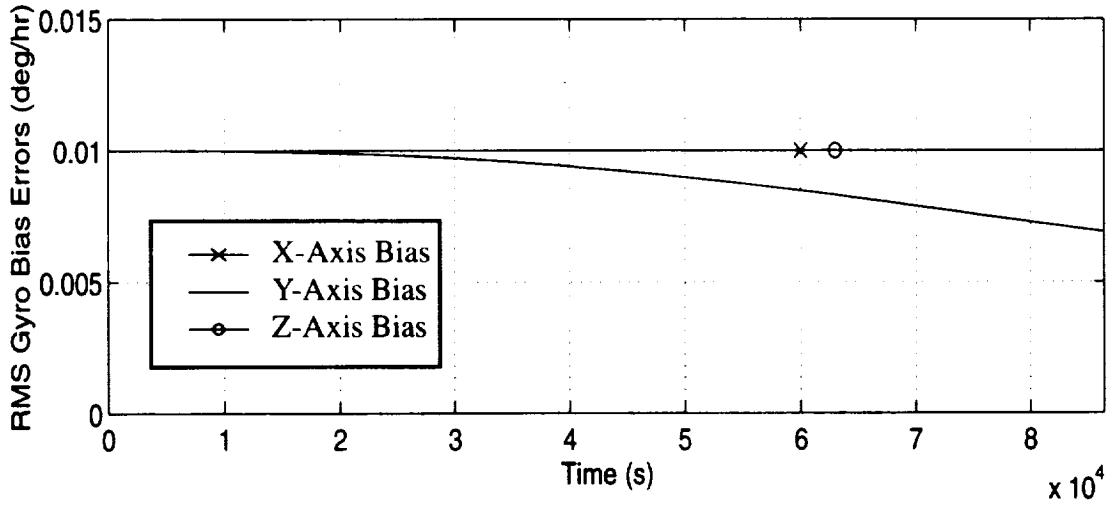


**Figure 5.7a Gyro Bias Errors**

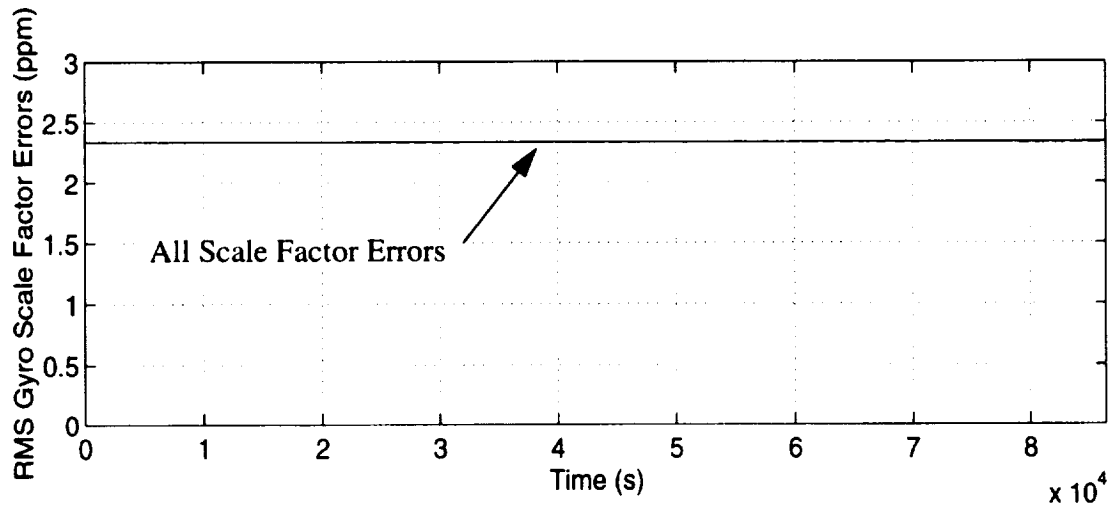


**Figure 5.7b Gyro Scale Factor Errors**

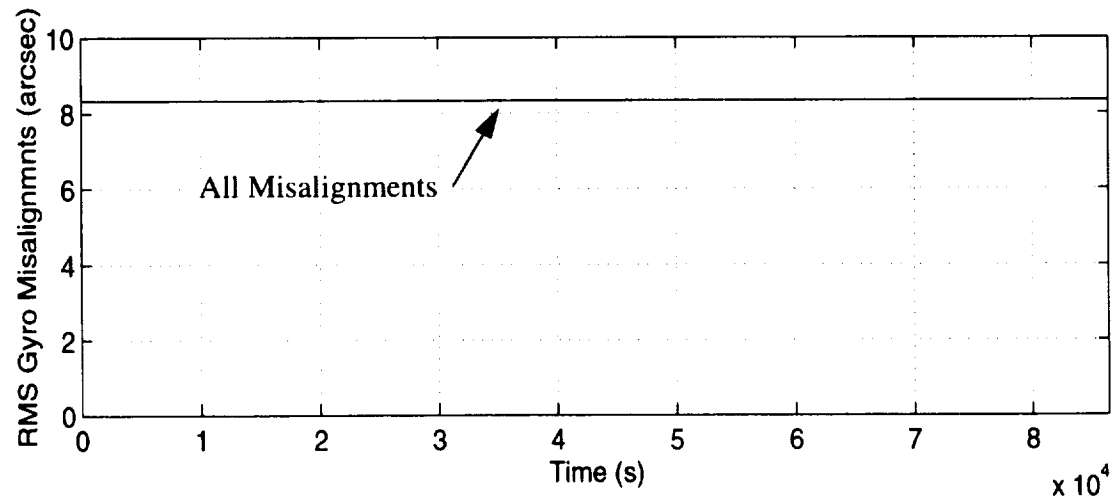


**Figure 5.7c Gyro Misalignments**



rotating about the body y-axis. This can be seen in Table 5.4, which shows the values of each component at the beginning and end of each run.

**Table 5.4 Gyroscope Errors**

Error	Component	$\sigma$ , t=0 seconds	$\sigma$ , t=86400 seconds
Gyro Bias (deg/hr)	X	0.0100	0.0100
	Y	0.0100	0.0069
	Z	0.0100	0.0100
Scale Factor Error (ppm)	X	2.3333	2.3333
	Y	2.3333	2.3313
	Z	2.3333	2.3333
Misalignment (arcsec)	$\gamma_{xy}$	8.3333	8.3333
	$\gamma_{xz}$	8.3333	8.3240
	$\gamma_{yx}$	8.3333	8.3333
	$\gamma_{yz}$	8.3333	8.3333
	$\gamma_{zx}$	8.3333	8.3287
	$\gamma_{zy}$	8.3333	8.3333

### 5.3 Results

In this section, the results of the individual runs for the different performance factors are presented. For each case, one factor at a time was varied from the nominal run presented in Table 5.2. Eight different performance factors were examined; these were summarized in Table 5.1.

### 5.3.1 Satellite Selection Routine

The attitude error magnitude was used to compare the performance of the satellite selection routines. The results are summarized in Table 5.5. These results show that for

**Table 5.5 Satellite Selection Routine Performance**

Run Description	Attitude Error Magnitude at t=6000 s (mrad)
SD GDOP	3.84
SD PYS	3.85
SD ADOP	3.93
SD Extended ADOP (nominal case)	3.84
DD GDOP	3.86
DD PYS	3.88
DD ADOP	3.87

applications with long mission durations, the satellite selection is not a very important factor in either the single difference or the double difference case.

### 5.3.2 Measurement Type

The factor varied in this case was the measurement type; the system performance when double difference measurements were used was compared to the nominal case, in which single differences were used. Since the RMS measurement noise on each single difference measurement is lower, by the square root of 2, than the RMS measurement noise on each double difference measurement, it was thought that if the path delays could be estimated well enough to counteract the increased noise, then better performance would be obtained using single difference measurements. Another advantage of single differences is that they are computationally simpler; double differ-

ences are not independent, and must be decorrelated before being incorporated. Also, one fewer satellite is needed for unique attitude determination. A disadvantage is that two more filter states are needed to estimate the path delays. Table 5.6 shows that there is very little difference in system performance due to the measurement type.

**Table 5.6 Measurement Types**

Measurement Type	Attitude Error RMS Magnitude at t=6000 sec (mrad)
SD	3.844
DD	3.847

### 5.3.3 Baseline Errors

The performance level is directly affected by how well the baselines are known, as shown in Figure 5.8. Large or moderate baseline errors are also responsible for the extremely long settling time of the system, as shown in Table 5.7, and Figure 5.8.

**Table 5.7 System Settling Times**

Baseline Errors (mm)	Settling Time (seconds)
0	10,000
1	15,000
5	50,000
10	80,000+

Estimation of the baseline length down to the noise floor is possible even with large initial error levels, as shown in Figure 5.9 and Figure 5.10. In each run considered in the section, the spacecraft was in the nominal attitude orientation, with the body x-axis

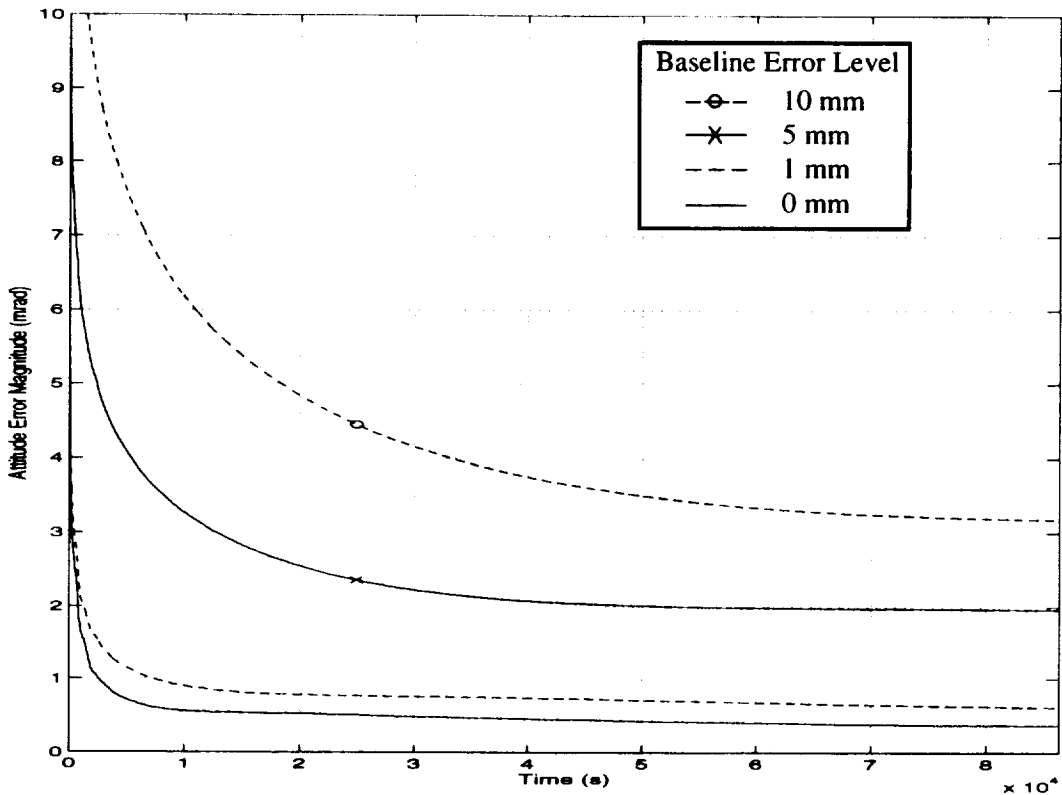


**Figure 5.8 Attitude Errors due to Different Baseline Error Levels**

pointed in the direction of velocity, and the vehicle rotating about the body y-axis. Therefore, baseline 1, which is along the body x-axis, sweeps out 360° during each orbit. The body z-axis errors of this baseline are difficult to distinguish from the orbital rotation, resulting in poor estimation of this quantity.

### 5.3.4 Multipath

Two facets of the multipath error were varied: the level of error, and the amount of correlation between the multipath errors received by the two baselines. The level of error was varied by changing the magnitude of the  $\sigma$  associated with each multipath error state. The amount of correlation was varied by changing the amount of multipath which was common to both baselines relative to the amount which was different for the two baselines.

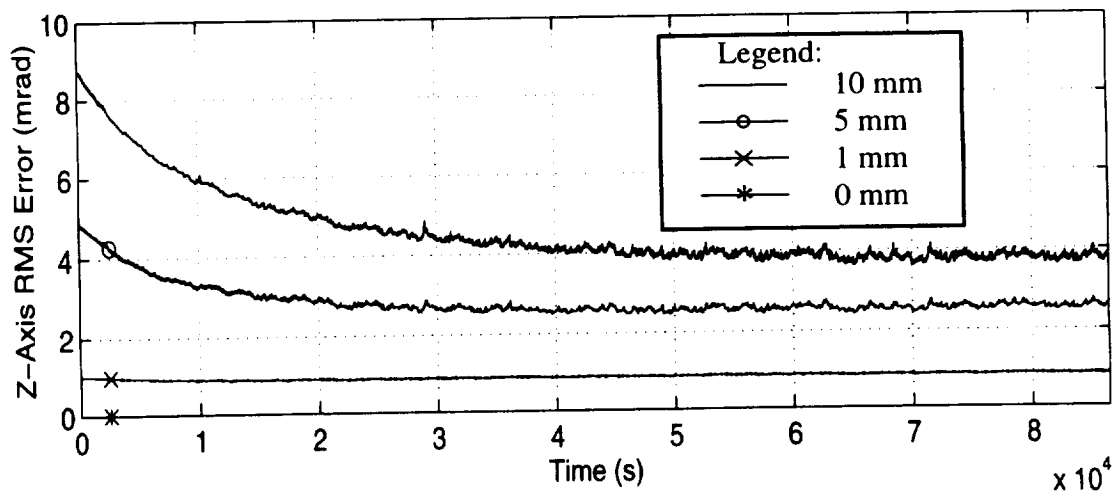
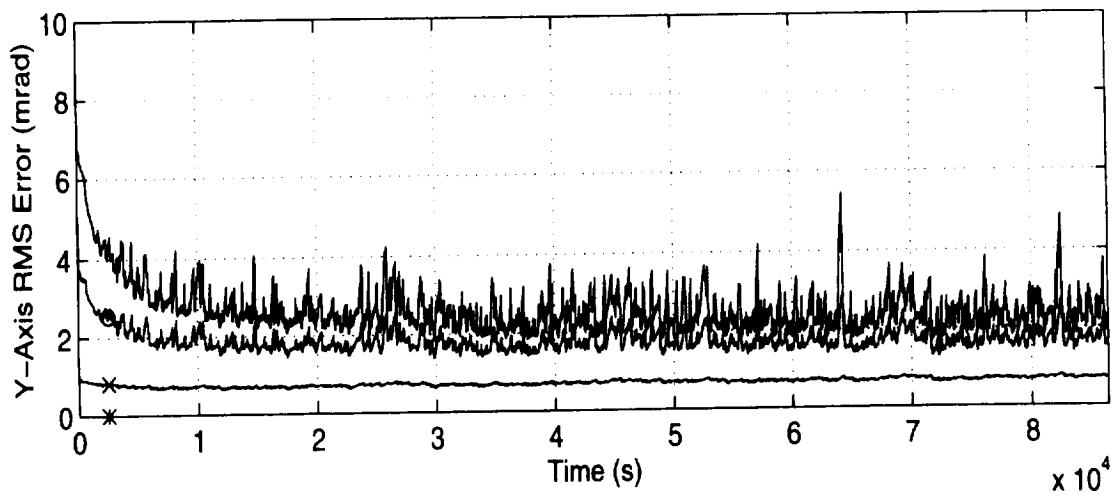
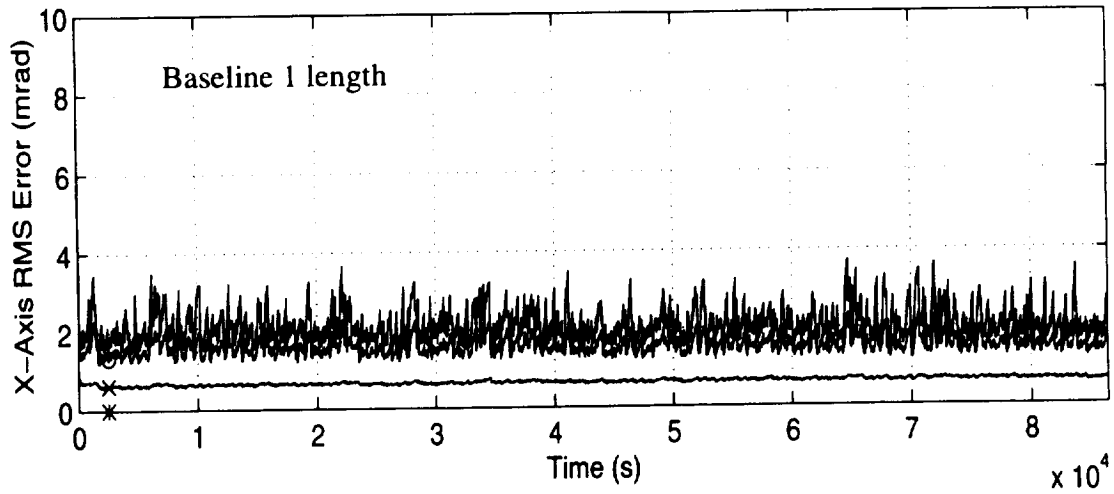


Figure 5.9 Baseline 1 Errors

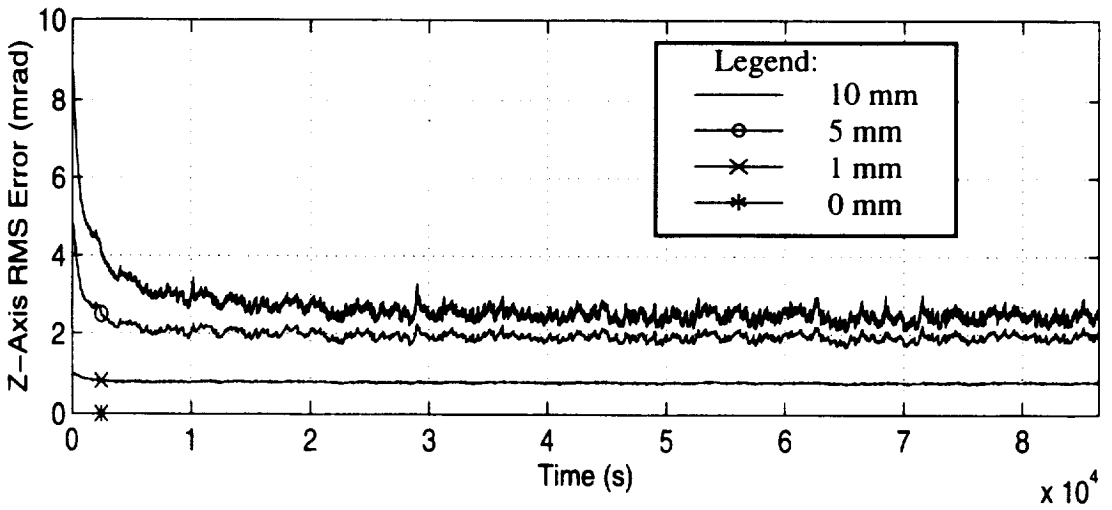
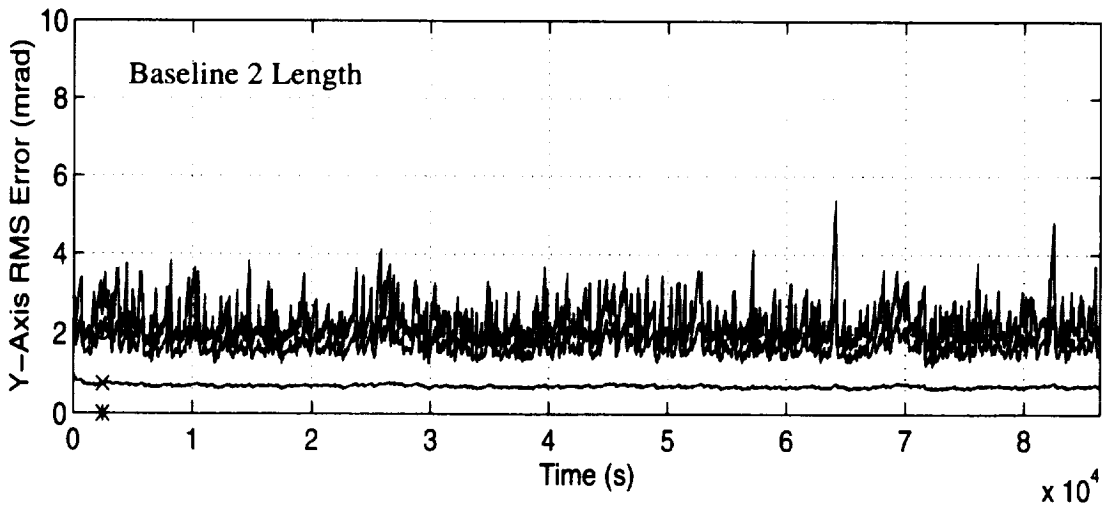
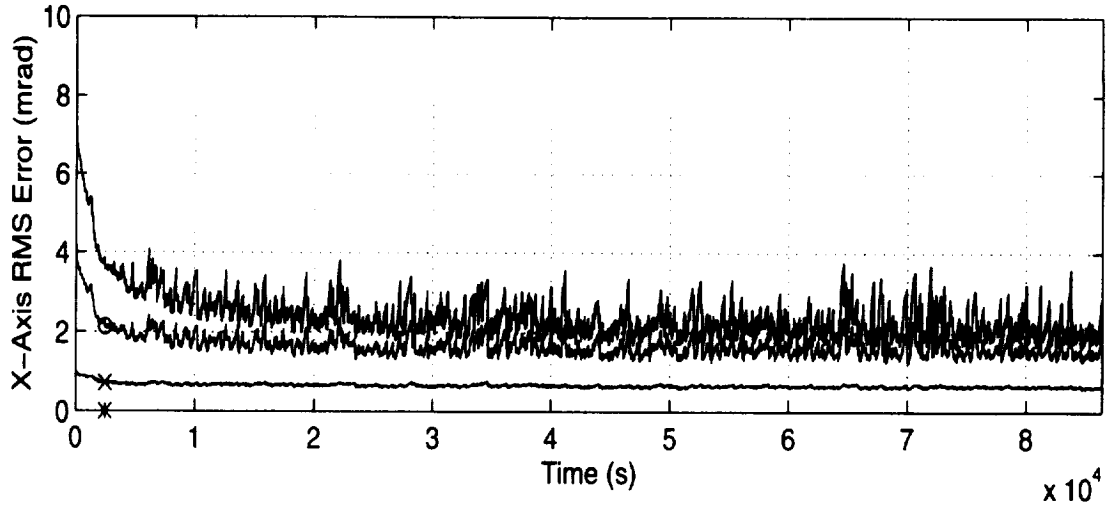


Figure 5.10 Baseline 2 Errors

### 5.3.4.1 Multipath Level

Multipath level was varied from 0 to 3.8 mm (nominal is 1.9 mm). As expected, the larger the multipath errors are, the less accurately the attitude can be estimated. (See Table 5.8.) However, there is only a small improvement in attitude error between the zero and nominal multipath cases. This indicates that the nominal multipath level modeled here does not contribute significantly to the attitude errors.

**Table 5.8 Multipath Level**

Multipath Level $\sigma$ , mm	Attitude Errors at t=6000 seconds (mrad)			
	X	Y	Z	RSS
0	1.14	3.40	1.15	3.76
1.9	1.20	3.45	1.20	3.84
3.8	1.30	3.56	1.30	4.01

### 5.3.4.2 Multipath Correlation

The amount of multipath correlation between the baselines was varied from 0-100%, using the relations

$$\sigma_i^2 = (1 - \rho) \sigma_m^2 \quad (5.2)$$

and

$$\sigma_c^2 = \rho \sigma_m^2 \quad (5.3)$$

where  $\sigma_m^2$  is the nominal variance of the multipath error,  $\sigma_i^2$  and  $\sigma_c^2$  are the variances of the independent and common multipath errors, respectively, and  $\rho$  is the correlation.

Slightly better attitude estimates are obtained when the multipath is highly correlated, as shown in Table 5.9. In this case, there are only four multipath processes

which are being estimated (one for each satellite), instead of eight or twelve as in the non-correlated or partially correlated cases. However, the table also shows that there is no significant difference in the accuracy of the attitude estimate due to the amount of multipath correlation.

**Table 5.9 Multipath Correlation**

Multipath Correlation	Attitude Errors at t=6000 seconds (mrad)			
	X	Y	Z	RSS
0%	1.20	3.45	1.20	3.85
50%	1.20	3.45	1.20	3.84
100%	1.19	3.45	1.19	3.83

### 5.3.5 Inclination

In a highly inclined orbit, it was thought that there may be fewer satellites visible than in an equatorial orbit or an orbit with the nominal inclination of 51.6°. If fewer satellites are available, then the performance of a GPS-based system could be limited in high inclination orbits. However, as Table 5.10 shows

**Table 5.10 Orbital Inclination**

Orbit Inclination	Attitude Error Magnitude at t=6000 seconds
0°	3.85
51.6°	3.84
90°	3.87



, there was no significant increase in the attitude errors for a polar orbit. In fact, there were not fewer satellites visible when the spacecraft was over a pole than at any other position in the orbit, as is shown in Figure 5.11.

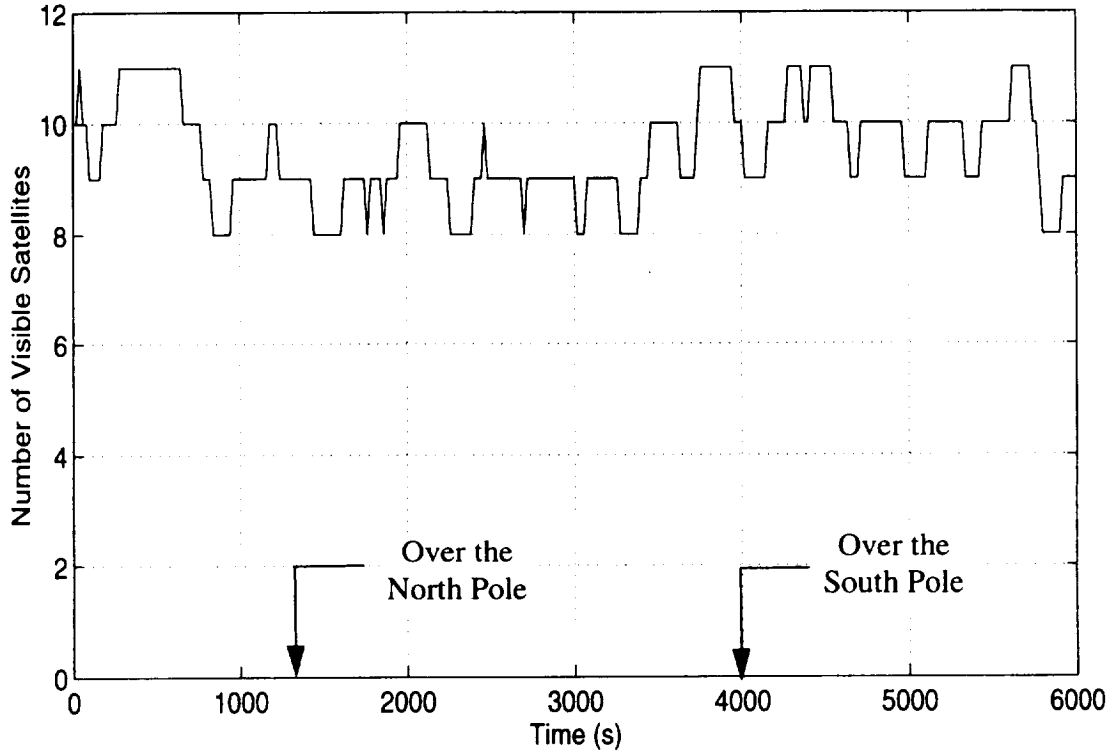


**Figure 5.11 Number of Satellites Visible During a Polar Orbit**

### 5.3.6 Attitude Hold

Three types of attitude hold were compared: LVLH, inertial, and attitude maneuvers. LVLH maintains the spacecraft orientation with respect to the earth; the x-axis points in the direction of velocity, the z-axis points away from the earth, and the y-axis is the cross track direction. This attitude corresponds to an aircraft flying nose forward, wings level around the earth. When the spacecraft was simulated as being in an inertial attitude hold, the initial attitude was the same as the LVLH case, but the inertial attitude remained constant throughout the run. In the maneuver case, the spacecraft again

started in the same initial attitude, and then performed a series of rotations, including one about each body axis. These rotations are recorded in Table 5.12.

The attitude errors were significantly less for the LVLH case than for the inertial case, as shown by the summary of results in Table 5.11, and in Figure 5.12. The main

**Table 5.11 Performance for Attitude Hold Cases**

Attitude Hold Type	Attitude Error (mrad)	
	t=7900	t=86400
LVLH	3.53	1.96
Inertial	5.27	3.10
Maneuvers	2.90	3.09

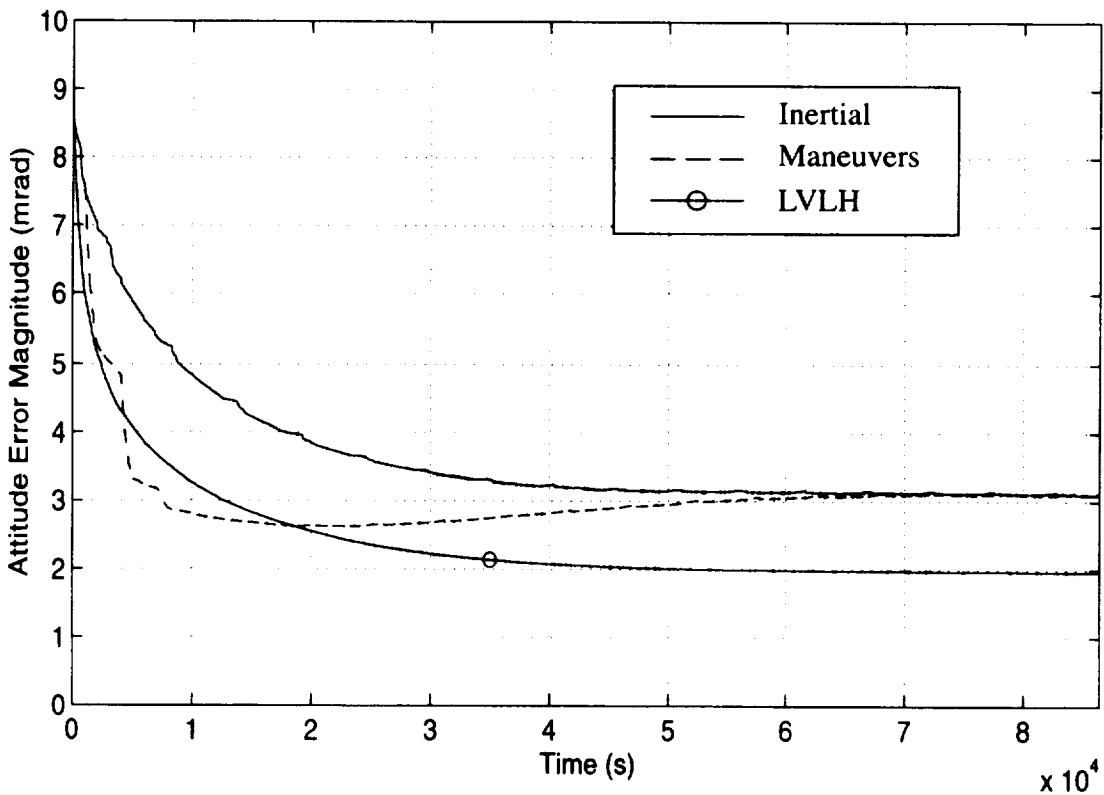


**Figure 5.12 Attitude Errors for all Attitude Hold Cases**

cause of this performance difference is that the rotation about the body y-axis which

occurs in the LVLH hold (due to the orbital rotation) allows errors in the baseline coordinates to be observable, and thus those errors can be estimated. This reasoning is supported by the results when maneuvers were performed which included rotations about each body axis. The performance results immediately after the conclusion of the maneuvers and at the end of the run are included in Table 5.11, and Figure 5.13 shows

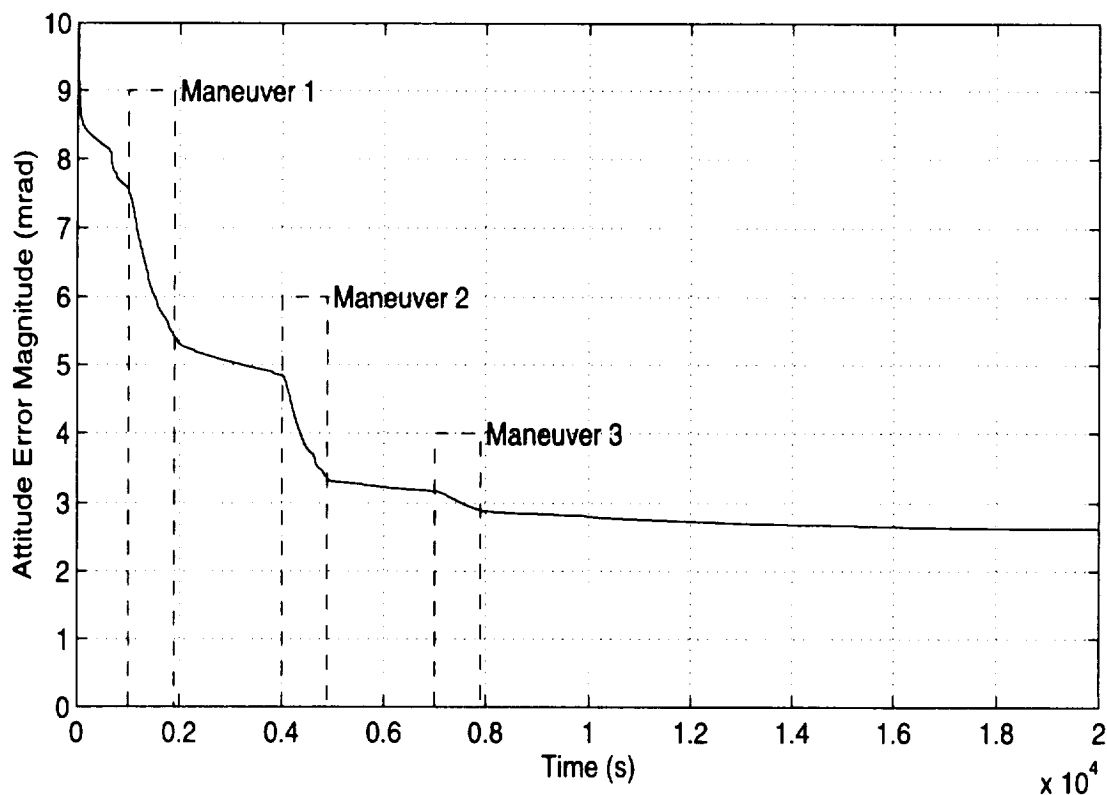


**Figure 5.13 Attitude Errors During Maneuvers**

the dramatic decrease in attitude error which occurs during each maneuver. However, as Figure 5.12 shows, this decrease is not maintained after the maneuvers have been completed.

When the spacecraft is in an inertial attitude hold, the earth blocks most of the satellites during a portion of each orbit. This results in an increase in attitude error, as can be seen in Figure 5.14. Figure 5.15 shows the number of satellites visible during this time.

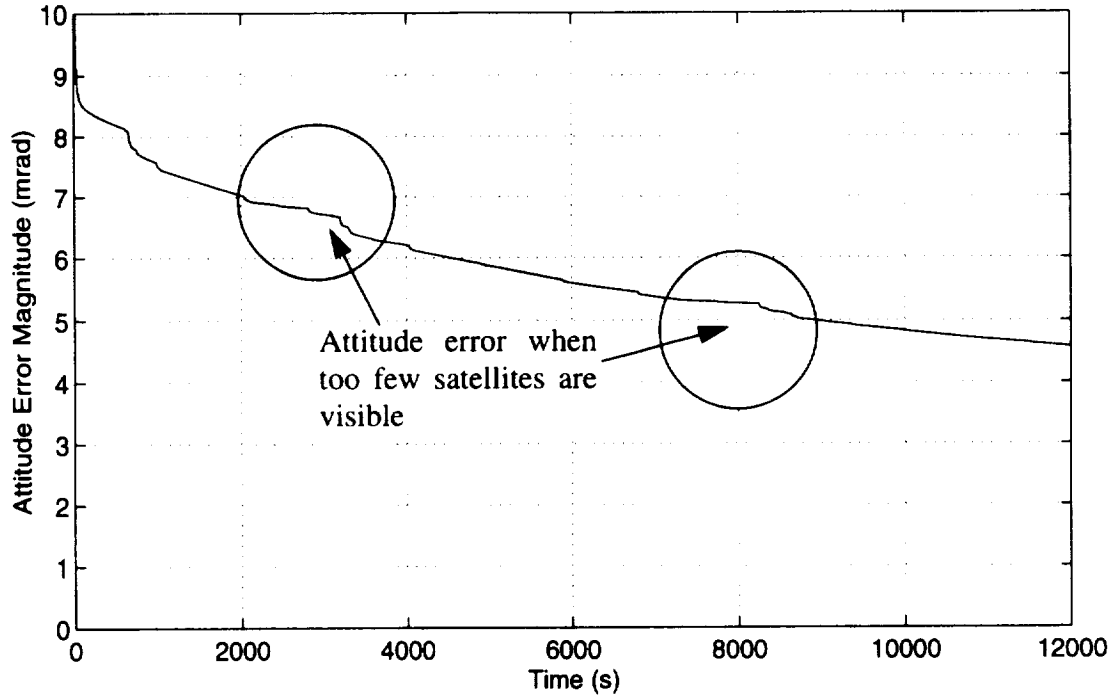


**Figure 5.14 Attitude Errors Caused by Loss of Satellite Visibility**

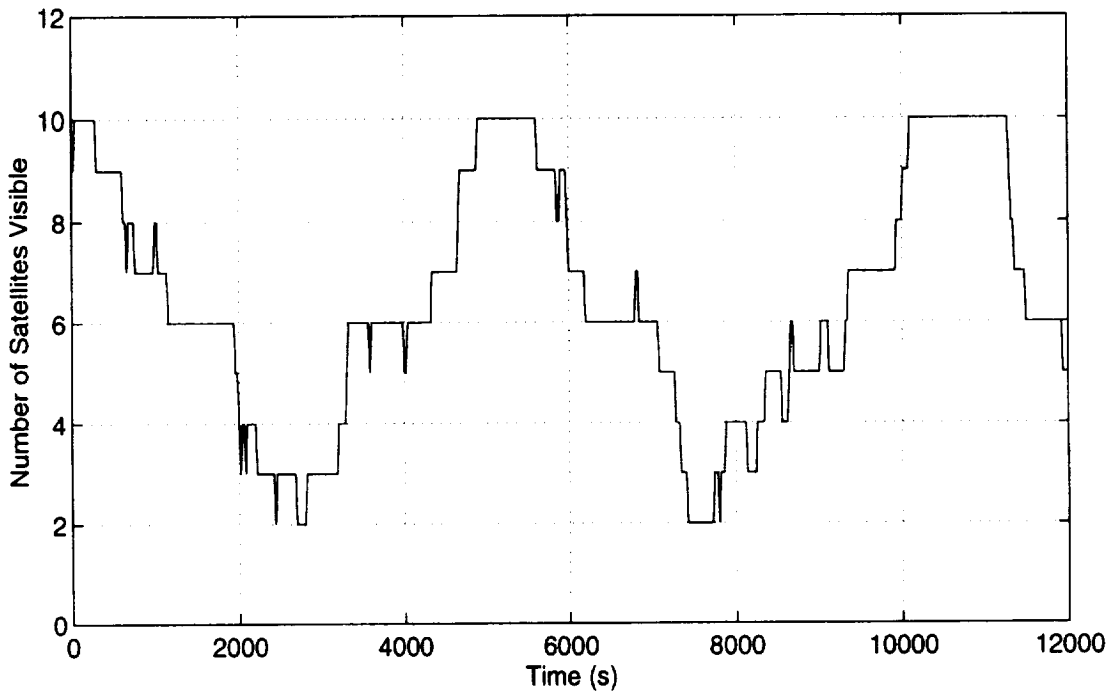


**Figure 5.15 Number of Satellites Visible While in an Inertial Attitude Hold**

**Table 5.12 Maneuver History**

Time Period (seconds)	Maneuver Description	
	Body Axis of Rotation	Rotation Rate (deg/hr)
0 - 1000	None	0.0
1000 - 1900	X	0.1
1900 - 4000	None	0.0
4000 - 4900	Y	0.1
4900 - 7000	None	0.0
7000 - 7900	Z	0.1
7900 - 86400	None	0.0

### 5.3.7 Gyroscope Quality

Two levels of gyroscope quality were modeled, a good quality gyro, which was similar to the gyro proposed for the Space Station, and a poor quality gyro. There was a marked degradation of performance when the poor quality gyroscopes were used; the results are summarized in Table 5.13, and Figure 5.16 shows the attitude errors.

**Table 5.13 Gyroscope Quality Results**

Gyro Quality	Attitude Error Magnitude at $t = 86400$ seconds (mrad)
Good	1.96
Poor	6.89

The reason that the gyro quality affects the long-term performance of the GPS/inertial system is that the baseline coordinates cannot be estimated as well with the bad gyros, as shown in Figure 5.17.

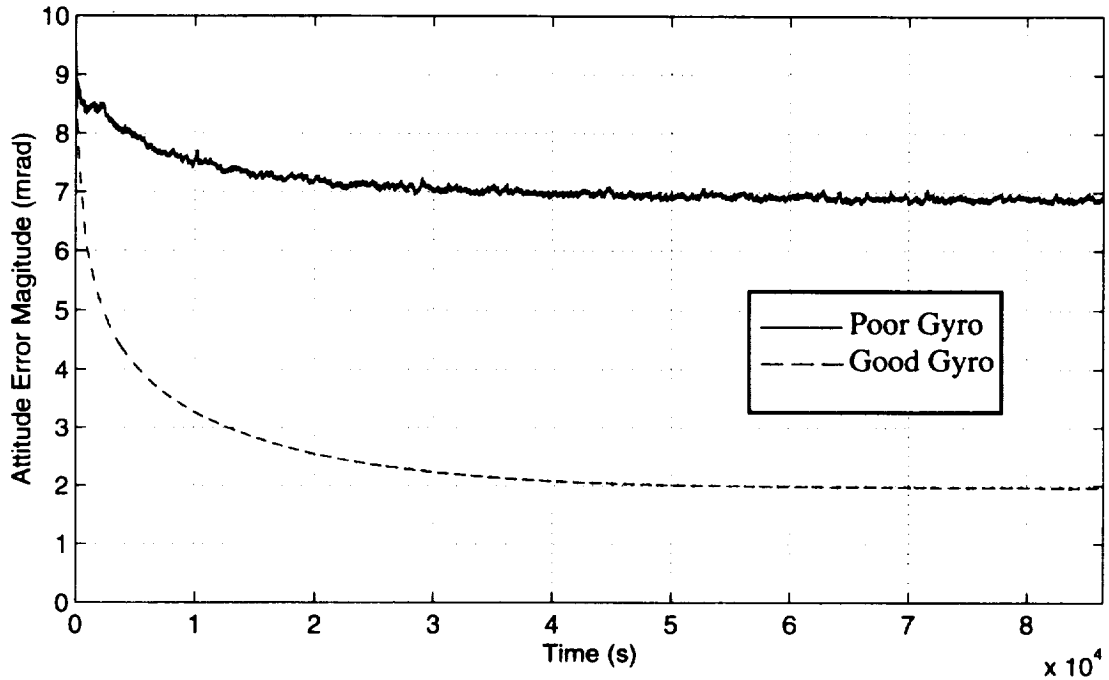


**Figure 5.16 Attitude Errors for Good and Poor Quality Gyroscope**

When the poor quality gyroscopes were used, it was possible to estimate the gyro bias. As Figure 5.18 shows, the estimate of gyro bias was improved by an order of

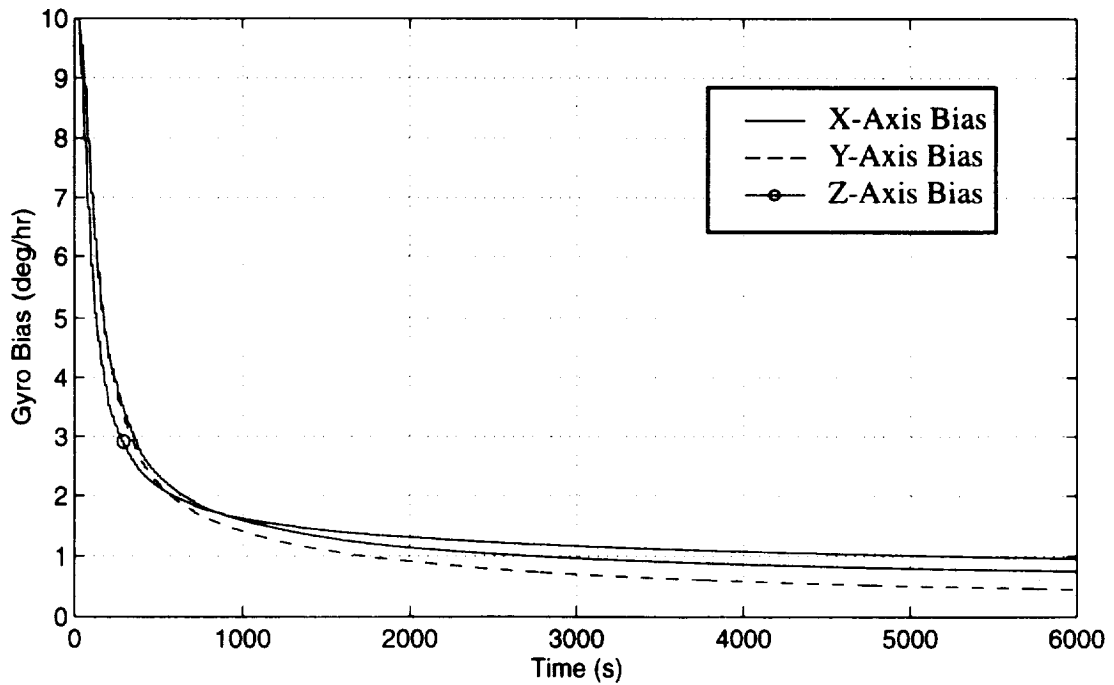


**Figure 5.18 Gyro Bias Estimation for a Poor Quality Gyroscope**

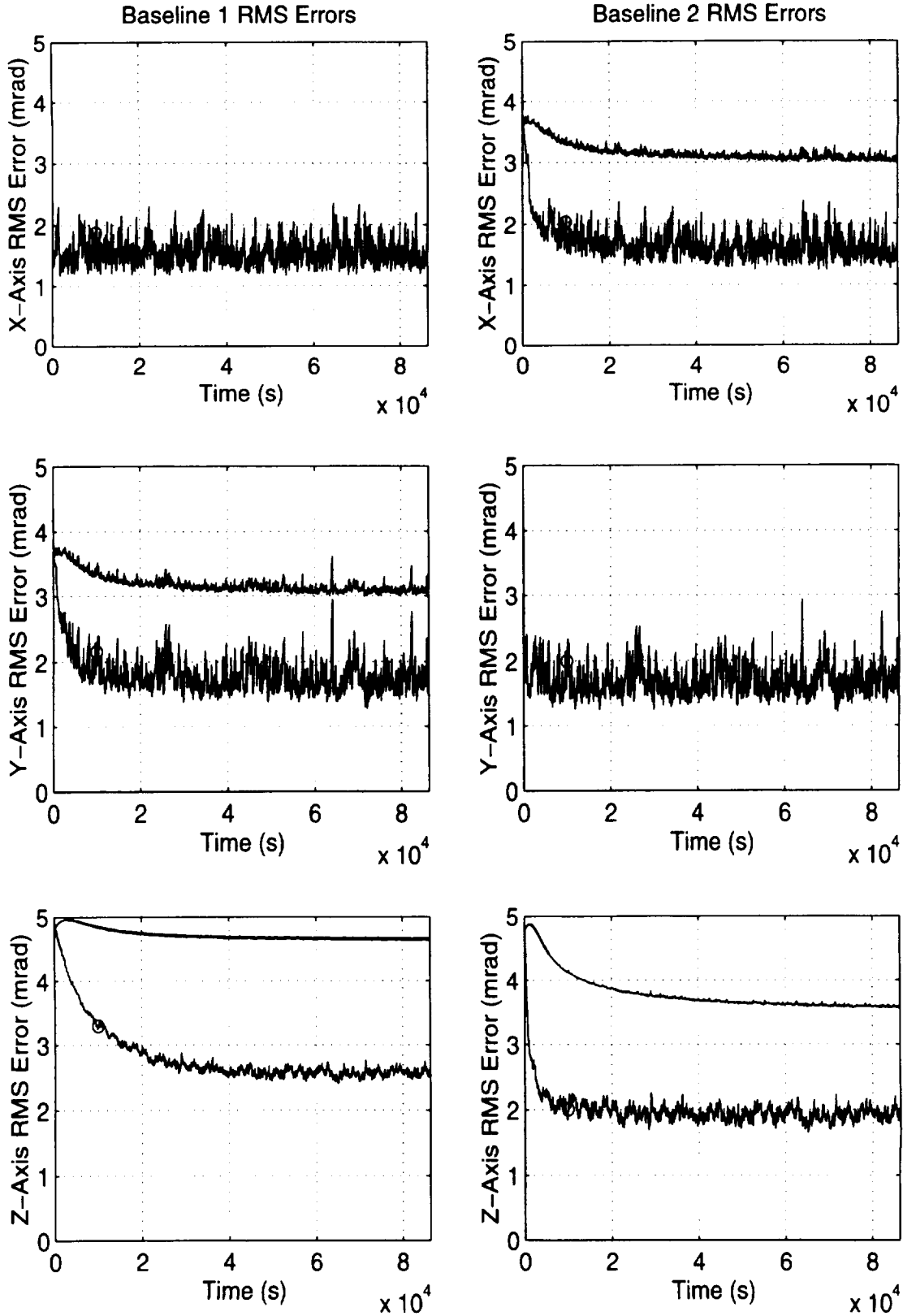


Figure 5.17 Comparison of Baseline Errors for Good and Poor Quality Gyros

magnitude over the course of the run, in effect improving a poor quality gyroscope to medium quality. The scale factor errors and the misalignments were not significantly reduced.



## Chapter 6

### Conclusions and Suggestions for Future Work

In this thesis, the performance of a GPS/inertial attitude determination system was investigated using a linear covariance analysis. The major error sources of both GPS interferometry and gyroscopes were modeled. A new figure of merit (Attitude Dilution of Precision, or ADOP) for satellite selection was presented and derived. Finally, the results of the linear covariance analysis were presented.

This chapter discusses the factors which enhance the accuracy of a GPS/inertial attitude determination system; the factors that limit accuracy; and finally, the factors that are not significant to the level of accuracy achieved. Also, suggestions for future research are made.

#### 6.1 Conclusions

The accuracy of the attitude determination estimate, given the error sources and levels, can be improved in two ways. First, measurements can be taken over a long period of time (approximately 15 hours). Second, maneuvers can be performed which increase the observability of the errors, and therefore allow for better and faster estimation.

However, the estimation of the baseline errors is a limiting factor for the attitude accuracy. If the RMS baseline flexures can be reduced, then not only will the attitude estimate accuracy improve, but the system will also reach its steady state performance more quickly, and lower quality gyros may be employed.

The simulation demonstrated that several factors which were thought to be potentially significant were in fact not very significant. For example, among the methods

considered, the method used for satellite selection did not significantly affect the errors. In addition, there was very little difference in results from the single difference vs. double difference measurements. The measurement type chosen will therefore depend on other factors, such as computational considerations, the number of satellites expected to be visible, and any limitations on the number of filter states which are available.

Finally, it was found that there is no loss of satellite visibility in high inclination orbits, and therefore orbital inclination does not significantly affect the attitude errors. The amount of multipath correlation also has very little bearing on the size of the errors. Increasing the amount of multipath results in only a slight increase in the RMS attitude error.

## **6.2 Future Work**

In this thesis, an error analysis was conducted using a linear covariance simulation. The next step in evaluating the performance of this system is to implement a Monte Carlo simulation. In this type of simulation, nonlinear effects could be included in the environment model, resulting in a more accurate model.

The GPS/inertial attitude determination system has the potential to be used for “fault detection,” i.e. to reject erroneous GPS measurements, a possibility that was not investigated here. Because of the high bandwidth of the gyroscopes, they could easily be used to detect cycle slip or an incorrect integer ambiguity.

In this analysis, baseline errors were modeled as exponentially correlated random variables. Because these errors were the most significant, it is important that they be properly characterized. In addition, performance may be improved by the development of multipath calibration techniques suitable for space vehicles.

## Appendix A

### Geometric Dilution of Precision (GDOP)

In Reference [16], Leick describes GDOP. The following is a summary of that discussion.

Generally, the parameters that are important to the positioning problem are

$$\{x_k, y_k, z_k, dt_k\} \quad (\text{A.1})$$

where  $x_k$ ,  $y_k$ , and  $z_k$  are the coordinates of receiver  $k$  in an Earth-centered, inertial reference system, and  $dt_k$  is the clock error of receiver  $k$ . The observable most often used for positioning is the pseudo range, which is a measure of the distance between the receiver and the satellite. The pseudo range equation for receiver  $k$  and satellite  $p$  is

$$\begin{aligned} P_k^p &= \sqrt{(x^p - x_k)^2 + (y^p - y_k)^2 + (z^p - z_k)^2} + c \cdot dt_k \\ &= \rho_k^p + c \cdot dt_k \end{aligned} \quad (\text{A.2})$$

where  $(x^p, y^p, z^p)$  are the coordinates of the satellite, and  $c$  is the speed of light. Note that Leick's notation uses a superscript to denote the satellites ("high in the sky"), and subscripts to denote a receiver on earth. The design matrix is formed by calculating the sensitivity of each pseudo range to each of the parameters listed in Equation (A.1):

$$A = \begin{bmatrix} \frac{x^1 - x_k}{\rho_k^1} & \frac{y^1 - y_k}{\rho_k^1} & \frac{z^1 - z_k}{\rho_k^1} & c \\ \frac{x^2 - x_k}{\rho_k^2} & \frac{y^2 - y_k}{\rho_k^2} & \frac{z^2 - z_k}{\rho_k^2} & c \\ \frac{x^3 - x_k}{\rho_k^3} & \frac{y^3 - y_k}{\rho_k^3} & \frac{z^3 - z_k}{\rho_k^3} & c \\ \frac{x^4 - x_k}{\rho_k^4} & \frac{y^4 - y_k}{\rho_k^4} & \frac{z^4 - z_k}{\rho_k^4} & c \end{bmatrix} \quad (A.3)$$

Then

$$(A^T A)^{-1} = \begin{bmatrix} \sigma_x^2 & \sigma_{xy} & \sigma_{xz} & \sigma_{xt} \\ \sigma_{yx} & \sigma_y^2 & \sigma_{yz} & \sigma_{yt} \\ \sigma_{zx} & \sigma_{zy} & \sigma_z^2 & \sigma_{zt} \\ \sigma_{tx} & \sigma_{ty} & \sigma_{tz} & \sigma_t^2 \end{bmatrix} \quad (A.4)$$

For terrestrial applications, the covariance matrix above is usually transformed to a local navigation frame. However, inertial coordinates were the most appropriate for the space application considered in this thesis. GDOP is then calculated as root sum of the diagonal elements of  $(A^T A)^{-1}$ , so that

$$GDOP = \sqrt{\text{trace} (A^T A)^{-1}} \quad (A.5)$$

## Appendix B

### Derivation of Pitch and Yaw Sensitivity Equations

The equations presented in the reference [14] for “Elevation Sensitivity” and “Azimuth Sensitivity” of a double difference measurement using satellites  $i$  and  $j$  are

$$\text{Elevation Sensitivity} = -\cos(\alpha_{ij} - \alpha_R) \cos\beta_{ij} \sin\beta_R + \sin\beta_{ij} \cos\beta_R \quad (\text{B.1})$$

$$\text{Azimuth Sensitivity} = \cos\beta_R \cos\beta_{ij} (-\cos\alpha_{ij} \sin\alpha_R + \sin\alpha_{ij} \cos\alpha_R) \quad (\text{B.2})$$

where the variables are:

$$\alpha_R = \text{antenna baseline azimuth}$$

$$\beta_R = \text{antenna baseline elevation}$$

$$\alpha_{ij} = \text{azimuth of vector to satellite (s)}$$

$$\beta_{ij} = \text{elevation of vector to satellite (s)}$$

These equations apply equally to the SD and DD cases, the only difference between the two being the vector to the satellite(s). In the SD case it is the LOS vector to the satellite, in the DD case, it is the difference of the unit LOS vectors. The satellite elevation and azimuth are shown in Figure B.1 for both the SD and DD cases.

In the orbital environment, “azimuth” and “elevation” are not well defined in reference to either the baselines or the satellites. Therefore, a local level frame was defined with the horizontal plane coincident with the antenna array plane, and the vertical direction the same as the antenna “look direction,” which is perpendicular to the antenna array plane.

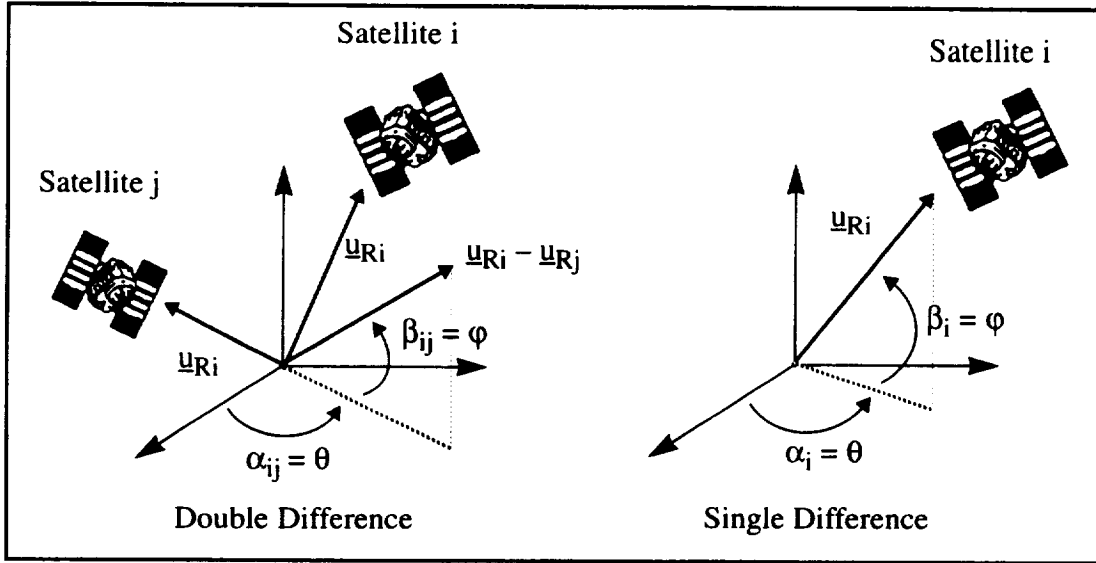


**Figure B.1 Satellite Elevation and Azimuth Angles for DD and SD Cases**

Then, baseline “elevation” was redefined to be baseline “pitch,” or rotation out of the antenna array plane. Baseline “azimuth” was redefined to be “yaw,” or rotation in the array plane. Since the local level frame is defined by the baseline location and direction,  $\alpha_R$  and  $\beta_R$  are identically zero. Satellite “azimuth” and “elevation” in the local level frame are simply the spherical coordinates of the satellite relative to the baseline, as shown in Figure B.1. Therefore, pitch sensitivity can be calculated from Equation (B.1) as

$$\begin{aligned}
 \text{Pitch Sensitivity} &= -\cos(\alpha_i - 0) \cos\beta_i \sin(0) + \sin\beta_i \cos(0) \\
 &= 0 + \sin\beta_i (1) \\
 &= \sin\beta_i
 \end{aligned} \tag{B.3}$$

and yaw sensitivity can be calculated from Equation (B.2) as

$$\begin{aligned}
 \text{Yaw Sensitivity} &= \cos(0) \cos\beta_i (-\cos\alpha_i \sin(0) + \sin\alpha_i \cos(0)) \\
 &= (1) \cos\beta_i ((0) + \sin\alpha_i (1)) \\
 &= \cos\beta_i \sin\alpha_i
 \end{aligned} \tag{B.4}$$

## Appendix C

### The Dynamics and Process Noise Matrices

Given the state vector  $\underline{x}^T = [\underline{\psi}^T \ \underline{\epsilon}^T \ \underline{\beta}^T \ \underline{\gamma}^T \ \delta b_1^T \ \delta b_2^T \ \underline{\xi}^T \ \rho_1 \ \rho_2]$ , then the dynamics matrix is

F =

$$\begin{bmatrix}
 (-\omega_B^1 \underline{x}) \ I_3 \ \begin{bmatrix} \omega_x & 0 & 0 \\ 0 & \omega_y & 0 \\ 0 & 0 & \omega_z \end{bmatrix} \ \begin{bmatrix} -\omega_z & \omega_y & 0 & 0 & 0 & 0 \\ 0 & 0 & \omega_z & -\omega_x & 0 & 0 \\ 0 & 0 & 0 & 0 & -\omega_y & \omega_x \end{bmatrix} & 0_3 & 0_3 & 0_{3 \times 12} & 0_{3 \times 1} & 0_{3 \times 1} \\
 0_3 & 0_3 & 0_3 & 0_{3 \times 6} & 0_3 & 0_3 & 0_{3 \times 12} & 0_{3 \times 1} & 0_{3 \times 1} \\
 0_3 & 0_3 & 0_3 & 0_{3 \times 6} & 0_3 & 0_3 & 0_{3 \times 12} & 0_{3 \times 1} & 0_{3 \times 1} \\
 0_3 & 0_3 & 0_3 & 0_{3 \times 6} & 0_3 & 0_3 & 0_{3 \times 12} & 0_{3 \times 1} & 0_{3 \times 1} \\
 0_3 & 0_3 & 0_3 & 0_{3 \times 6} & (-\frac{1}{\tau_b}) I_3 & 0_3 & 0_{3 \times 12} & 0_{3 \times 1} & 0_{3 \times 1} \\
 0_3 & 0_3 & 0_3 & 0_{3 \times 6} & 0_3 & (-\frac{1}{\tau_b}) I_3 & 0_{3 \times 12} & 0_{3 \times 1} & 0_{3 \times 1} \\
 0_{12 \times 3} & 0_{12 \times 3} & 0_{12 \times 3} & 0_{12 \times 6} & 0_{12 \times 3} & 0_{12 \times 3} & (-\frac{1}{\tau_\xi}) I_{12} & 0_{12 \times 1} & 0_{12 \times 1} \\
 0_{1 \times 3} & 0_{1 \times 3} & 0_{1 \times 3} & 0_{1 \times 6} & 0_{1 \times 3} & 0_{1 \times 3} & 0_{1 \times 12} & (-\frac{1}{\tau_\rho}) & 0 \\
 0_{1 \times 3} & 0_{1 \times 3} & 0_{1 \times 3} & 0_{1 \times 6} & 0_{1 \times 3} & 0_{1 \times 3} & 0_{1 \times 12} & 0 & (-\frac{1}{\tau_\rho})
 \end{bmatrix}$$

The continuous process noise matrix is







$$Q_{k\xi} = \begin{bmatrix} \sigma_{\xi}^2 (1 - e^{-2dt/\tau_{\xi 1}}) & 0 & 0 & 0 \\ 0 & \sigma_{\xi}^2 (1 - e^{-2dt/\tau_{\xi 2}}) & 0 & 0 \\ 0 & 0 & \sigma_{\xi}^2 (1 - e^{-2dt/\tau_{\xi 3}}) & 0 \\ 0 & 0 & 0 & \sigma_{\xi}^2 (1 - e^{-2dt/\tau_{\xi 4}}) \end{bmatrix} \quad (\text{C.9})$$

and

$$Q_{kp1} = Q_{kp2} = \sigma_p^2 (1 - e^{-2dt/\tau_p}) \quad (\text{C.10})$$

# Appendix D

## Derivation of the Sensitivity Vectors

### D.1 Single Difference Case

The sensitivity vectors for the baseline errors and path delays can be calculated directly from the measurement equation; their derivations follow in Section D.1.1. The sensitivity for the attitude errors is more easily obtained by differencing the actual and predicted measurement. The attitude error sensitivity is derived in Section D.1.2.

#### D.1.1 Baseline Errors and Path Delays

The measurement equation is (from Equation (3.7))

$$SD = \lambda \left( n + \frac{\Delta\phi}{2\pi} \right) + pd = (\mathbf{u}_R^I)^T \mathbf{C}_B^I \mathbf{b}^B + pd$$

Since the sensitivity of the baseline errors is the same as the sensitivity to the baseline coordinates,  $\mathbf{h}_{\delta\mathbf{b}}^T$  is simply the partial derivative of the measurement with respect to  $\mathbf{b}$ , given by

$$\mathbf{h}_{\delta\mathbf{b}}^T = (\mathbf{u}_R^I)^T \mathbf{C}_B^I \quad (\text{D.1})$$

Likewise, the scalar sensitivity for each path delay is

$$h_{pd} = 1 \quad (\text{D.2})$$

Obviously, a single difference measurement is only sensitive to the baseline errors and path delay which are associated with the baseline which was used for the measurement.

#### D.1.2 Attitude Errors

In general (from Equation (4.13))

$$\begin{aligned}
q_{\text{meas}} &= \mathbf{h}^T \mathbf{x} + \mathbf{y} \\
q_{\text{pred}} &= \mathbf{h}^T \hat{\mathbf{x}}
\end{aligned} \tag{D.3}$$

and therefore

$$\begin{aligned}
\delta q &= q_{\text{meas}} - q_{\text{pred}} \\
&= -\mathbf{h}^T \delta \mathbf{x} + \mathbf{y}
\end{aligned} \tag{D.4}$$

Omitting measurement noise sources,

$$\begin{aligned}
q_{\text{meas}} &= \lambda \left( n + \frac{\Delta \phi}{2\pi} \right) + pd \\
&= (\mathbf{u}_R^I)^T \mathbf{C}_B^I \mathbf{b}^B + pd
\end{aligned} \tag{D.5}$$

and

$$q_{\text{pred}} = (\mathbf{u}_R^I)^T \hat{\mathbf{C}}_B^I \hat{\mathbf{b}}^B \tag{D.6}$$

Therefore,

$$\delta q = (\mathbf{u}_R^I)^T (\mathbf{C}_B^I \mathbf{b}^B - \hat{\mathbf{C}}_B^I \hat{\mathbf{b}}^B) + pd \tag{D.7}$$

By definition

$$\begin{aligned}
\hat{\mathbf{b}}^B &= \mathbf{b}^B + \delta \mathbf{b}^B \\
\hat{\Psi}^B &= \underline{\Psi}^B + \delta \underline{\Psi}^B
\end{aligned} \tag{D.8}$$

and

$$\begin{aligned}
\hat{\mathbf{C}}_B^I &= (\mathbf{I} + \hat{\Psi}^I \mathbf{x}) \mathbf{C}_B^I (\mathbf{I} - \underline{\Psi}^B \mathbf{x}) \\
&= \mathbf{C}_B^I (\mathbf{I} + \hat{\Psi}^B \mathbf{x} - \underline{\Psi}^B \mathbf{x}) \\
&= \mathbf{C}_B^I (\mathbf{I} + \delta \underline{\Psi}^B \mathbf{x})
\end{aligned} \tag{D.9}$$

where  $\underline{\Psi}\mathbf{x}$  is the cross product matrix form of the indicated vector. So,

$$\begin{aligned}
\delta q &= (\underline{u}_R^1)^T C_B^1 (\underline{b}^B - (I + \delta \underline{\Psi}^B \mathbf{x}) (\underline{b}^B + \delta \underline{b}^B)) + p d \\
&= (\underline{u}_R^1)^T C_B^1 (\underline{b}^B - \underline{b}^B - \delta \underline{b}^B - \delta \underline{\Psi}^B \mathbf{x} \underline{b}^B) + p d \\
&= (\underline{u}_R^1)^T C_B^1 (-\delta \underline{b}^B + \underline{b}^B \mathbf{x} \delta \underline{\Psi}^B) + p d
\end{aligned} \tag{D.10}$$

As with the baseline sensitivity,  $\mathbf{h}_\Psi^T$  is the same as  $\mathbf{h}_{\delta \Psi}^T$ , so

$$\mathbf{h}_\Psi^T = -(\underline{u}_R^1)^T C_B^1 (\underline{b}^B \mathbf{x}) \tag{D.11}$$

## D.2 Double Difference Case

As stated in Chapter 4, double difference measurement sets are decorrelated before being incorporated sequentially. Section D.2.1 describes the sensitivity vector of the actual measurement, and Section D.2.2 describes the transformation which decorrelates the measurements.

### D.2.1 Sensitivity Vectors

The sensitivity vectors for the baseline and attitude errors are the same as in the single difference case, with the exception that the LOS difference,  $(\underline{u}_{R1}^1 - \underline{u}_{R2}^1)$ , is substituted for the LOS,  $\underline{u}_R^1$ . Therefore,

$$\mathbf{h}_{\delta b}^T = (\underline{u}_{R1}^1 - \underline{u}_{R2}^1)^T C_B^1 \tag{D.12}$$

and

$$\mathbf{h}_\Psi^T = -(\underline{u}_{R1}^1 - \underline{u}_{R2}^1)^T C_B^1 (\underline{b}^B \mathbf{x}) \tag{D.13}$$

The path delays cancel out in double difference measurements, therefore, the path delay sensitivity is zero.

## D.2.2 Measurement Noise Decorrelation

As explained in Section 4.1, R must be diagonal in order to do sequential processing. Any full square matrix can be transformed to a diagonal one using an eigenvalue/eigenvector decomposition. That is, given any nxn matrix R

$$\mathbf{T}^T \mathbf{R} \mathbf{T} = \begin{bmatrix} \lambda_1 & & 0 \\ & \lambda_2 & \\ 0 & & \dots \\ & & & \lambda_n \end{bmatrix} \quad (\text{D.14})$$

where  $\lambda_i$  are the eigenvalues of R, and the columns of T are the eigenvectors of R. T is called the modal matrix.

A correlated batch of measurements with the sensitivity vectors forming the columns of H, and  $\langle \mathbf{y} \cdot \mathbf{y}^T \rangle = \mathbf{R}$  (not diagonal) is represented by Equation (4.9). An uncorrelated set of measurements which contain the same information is given by

$$\mathbf{z}' = \mathbf{T}^T \mathbf{z} = \mathbf{T}^T \mathbf{H} \mathbf{x} + \mathbf{T}^T \mathbf{y} \quad (\text{D.15})$$

The measurement set defined by Equation (D.15) is uncorrelated because

$$\begin{aligned} \langle \mathbf{T}^T \mathbf{y} \cdot \mathbf{y}^T \mathbf{T} \rangle &= \mathbf{T}^T \langle \mathbf{y} \cdot \mathbf{y}^T \rangle \mathbf{T} \\ &= \mathbf{T}^T \mathbf{R} \mathbf{T} \end{aligned} \quad (\text{D.16})$$

and  $\mathbf{T}^T \mathbf{R} \mathbf{T}$  is a diagonal matrix, as shown in Equation (D.14).

The sensitivity vectors,  $\mathbf{h}^T$ , for the measurement  $\mathbf{z}'$  are then the rows of  $\mathbf{T}^T \mathbf{H}$ .

## References

- [1] Axelrad, P., Chesley, B., "Performance Testing of a GPS Based Attitude Determination System", AIAA-93-3787-CP.
- [2] Brown, A. K., "Interferometric Attitude Determination Using the Global Positioning System", MIT Master of Science Thesis, August, 1981.
- [3] Brown, R., Ward, P., "A GPS Receiver with Built-in Precision Pointing Capability", Texas Instruments, Inc., CH2811, August, 1990.
- [4] Cohen, C. E., Parkinson, B. W., "Mitigating Multipath Error in GPS Based Attitude Determination", AAS 91-024.
- [5] Diefes, D., et al., "Dynamic GPS Attitude Determining System (ADS) for Marine Applications—Concept Design and Developmental Test Results", *Proceedings of the National Technical Institute of Navigation*, January 20–22, 1993.
- [6] Ellis, J. F., Creswell, G. A., "Interferometric Attitude Determination with the Global Positioning System", *Journal of Guidance and Control*, Nov-Dec, 1979, Vol. 2, No. 6, Article No. 78-1250R.
- [7] Ferguson, K., et al., "Three-Dimensional Attitude Determination with the Ashtech 3DF 24-Channel GPS Measurement System", Ashtech, Inc., Sunnyvale, CO, 94086.
- [8] Gelb, A., *Applied Optimal Estimation*, The M.I.T. Press, Cambridge, MA, 1974.
- [9] Grass, F., Braasch, M. S., "GPS Interferometric Attitude and Heading Determination: Flight Test Results", 47th ION Annual Meeting, Williamsburg, VA, June 10–12, 1991.
- [10] Hatch, R., "Ambiguity Resolution in the Fast Lane", *Proceedings of the Second International Technical Meeting of the Institute of Navigation's Satellite Division*, Colorado Springs, CO, 1989.
- [11] Jurgens, R., "Realtime GPS Azimuth Determining System", *Proceedings of the National Technical Institute of Navigation*, January 23-25, 1990.
- [12] Jurgens, R., et al., "Measurement of Errors in GPS Attitude Determining Systems", *Proceedings of ION GPS-92 Fifth International Technical Meeting of the Satellite Division, Institute of Navigation*, September 16-18, 1991.
- [13] Jurgens, R., Rodgers, C., "Advances in GPS Attitude Determining Technology as Developed for the Strategic Defense Command", Adroit Systems, Inc.
- [14] Keierleber, K., Maki, S., "Attitude Determination for Space Transfer Vehicles Using GPS", *Proceedings of the National Technical Institute of Navigation*, January 22-24, 1991.
- [15] Langley, R. B., "The GPS Observables", *GPS World*, April 1993.
- [16] Leick, A., *GPS Satellite Surveying*, John Wiley & Sons, Inc., New York, NY, 1990.
- [17] Lightsey, E. G., Cohen, C. E., Parkinson, B. W., "Application of GPS Attitude Determination to Gravity Gradient Stabilized Spacecraft", AIAA-93-3788-CP.

- [18] Martin-Neira, M., Lucas, R., "Using GPS to Determine the Attitude of a Spacecraft", *GPS World*, March, 1993.
- [19] Maybeck, P., *Stochastic Models, Estimation, and Control Volume I*, Academic Press, Inc., San Diego, CA, 1979.
- [20] McMillan, J. C., "Interferometric GPS Attitude: A Stochastic Error Model", Defence Research Establishment Ottawa, Report No. 1168, February, 1993.
- [21] Miller, B. L., et al., *A Kalman Filter Implementation for Dual-Antenna GPS Receiver and an Inertial Navigation System*.
- [22] Rath, J., Ward, P., "Attitude Estimation Using GPS", *Proceedings of the National Technical Institute of Navigation*, January 23-26, 1984.
- [23] Satz, H., Cox, D., "GPS Inertial Attitude Estimation via Carrier Accumulated-Phase Measurements", *Navigation: Journal of The Institute of Navigation*, Vol. 38, No. 3, Fall 1991.
- [24] Upadhyay, T., Cotterill, S., Deaton, A. W., "Autonomous GPS/INS Navigation Experiment for Space Transfer Vehicle", *IEEE Transactions on Aerospace and Electronic Systems*, Vol. 29, No. 3, July, 1993.
- [25] "Codeless GPS Attitude Determination System", ITHACO Technical Services, Lanham, MD 20706, August 12, 1992.
- [26] "GPS Attitude Sensing Tested", *Aviation Week and Space Technology*, November 30, 1992.